NTNU

Norwegian University of
Science and Technology

Fixed Speed Electric Motor Drives for LNG Refrigeration Compressors.

Back-to-Back Starting Methods and Grid Consequences.

Hallvard Breistein

Master of Science in Energy and Environment
Submission date: June 2009
Supervisor: Tom F. Nestli, ELKRAFT

Norwegian University of Science and Technology
Department of Electrical Power Engineering

Problem Description

1. Perform a literature study into the subject.
2. Investigate the feasibility of low-, partial frequency and soft starting of generator and compressor drive system connected Back-to-Back.
3. Perform laboratory tests of a scaled version of at least one of the aforementioned starting schemes.
4. Validate simulation model for Back-to-Back start-up using parameters from laboratory, and study the physical effects that could prevent starting.
5. Perform simulations on full scale model using actual parameters.
6. Investigate the consequences of fixed speed drives in LNG plant grid.
7. Conclude on the technical feasibility and advantages/drawbacks of fixed speed LNG.

Assignment given: 15. January 2009
Supervisor: Tom F. Nestli, ELKRAFT

Preface

This masters thesis is a feasibility study conducted on behalf of the Aker Solutions subsidiary Aker Engineering & Technology. It is based on an idea for a revised electrical system for LNG plants. Thanks is owed to Ole-Johan Bjerknes who's think-outside-the-box mindset provided the problem description on behalf of Aker Solutions. He has been very helpful in providing industrial know-how, representative parameters, and relevant suggestions.

I would also like to thank my superviser Prof. 2. Tom Fagernes Nestli for his academic guidance and input. Thanks also goes to Phd. Temesgen Hailesellasie for his interest in my problems. I am deeply indebted to Bård Almaas and Thor Lohse at the service lab, without whom my experimental work surely would have stranded.

Abstract

Experimental studies as well as simulations have been performed on the Back-to-Back starting schemes low frequency-, partial frequency-, and soft -start-up. A Back-to-Back configuration of two synchronous machines has been established in the laboratory, upon which parameter estimation and start-up experiments have been performed. Extensive

parameter estimation was conducted in order to, as accurately as practically possible, replicate the laboratory machines in a simulation model that was constructed in the pre-project. This was done in order to verify the validity of the simulation model. Studies into the effects of inductance interconnecting the machines were made in the laboratory and in the simulation model. Effects of resistance and inertia were studied in the simulation model. It is concluded that the simulation model appears to be as reliable as is its input parameters. Discrepancies were found in line voltages, due to weaknesses in the implementation of field current replication. Full scale simulations using ABB

Motorformer parameters obtained from StatoilHydro were performed in the simulation model, featuring low frequency- and soft -staring. The effects of an interconnecting cable were studied. It is concluded that low frequency starting appears to be most reliable and least violent starting method. However, it might be limited by the availability of a turbine. This is not the case for soft starting, which has a lower starting capability and is more violent to the motor damper- and field windings. Low frequency start-up is hence the recommended starting method of the ones studied. Dynamic short

circuit simulations were done on a fixed speed LNG-facility. The fixed speed alternative appears to be more stable when responding to a short circuit. This is because the motors contribute to upholding the voltage during a fault by delivering reactive power to the short circuit, and because the motors do not loose all torque as is the case for LCI drives when the voltage dip exceeds 20%. Further work is needed in up-scaling the

experiments. A sophisticated simulation model should be established and its validity tested on the up-scaled experiments. Preliminary custom design of machines should be initiated depending on what starting scheme is chosen. Custom machine parameters should then be used in full scale simulation using the more sophisticated model.

Contents

List of Tables

List of Figures

Nomenclature

- l - Inductance
- λ - Flux linkeage
- Φ - Magnetic flux
- e - Internally induced voltage
- $\hat{E}$ - Voltage phasor
- E - Magnitude of voltage
- $|Z|$ - Magnitude of impedance
- ϕ - Current phase angle
- δ - Internally induced voltage phase angle - Power angle
- ω - Rotational speed rad/s
- β_z - Angle of impedance
- α - Ratio of compressor mechanical power to turbine mechanical power.
- η - Efficiency
- f - Frequency

Acronyms

- LNG - Liquefied Natural Gas
- GT - Gas turbine
- E-LNG - Electric - LNG
- EPC - Engineering procurement and construction
- CAPEX - Capital expenditure
- OPEX - Operational expenditure
- LCI - Load commutated inverter
- MMF - Magnetomotive force
- DOL - Direct on line

Chapter 1

Background and prior work.

1.1 Introduction

In the following an account will be made of the background for this thesis. The objectives of the work be presented and placed into an industrial context.

1.1.1 Electric LNG

Traditionally Liquified Natural Gas (LNG) facilities have used gas turbines (GTs) to drive their refrigeration compressors. The GT is then mounted on the same shaft as the compressor without any gear in between [1]. In later years the talk in the industry has been on electric LNG facilities, a discourse culminating with StatoilHydro's Snøhvit facility at Melkøya by Hammerfest, Norway.

One of the main reasons for a shift towards electric drivers is fewer maintenance hours per year. According to Shu et. al., in traditional LNG-facilities the scheduled maintenance downtime for the Frame 7 or -9 gas turbines is 270 hours per year. This is more than five times that of the next most demanding component, i.e. the compressors themselves [1]. When the GT is fitted to the compressor shaft, GT downtime will lead to production halt. For the direct driven example case studied in [1], the production availability due to less maintenance was increased by 2.9% when compared to electric LNG. This corresponds to $210 million over the entire life cycle of the facility. Kauffman et. al. concludes that a shift from direct GT drive system with electric helper motors, hybrid drive, to only electric drivers, would entail a minimum of ten additional on-stream days per year. The annual production benefit from this is estimated to $29.6 million on a 5 mtpa train [2].

In addition to being a high maintenance component, the high powered Frame 7 and -9 GTs have long delivery times. Therefore practice has been to order the GTs before the final investment decision has been made [1]. The centralized power plant that drives the electric drivers can use smaller GTs with shorter delivery times. The latter is also true

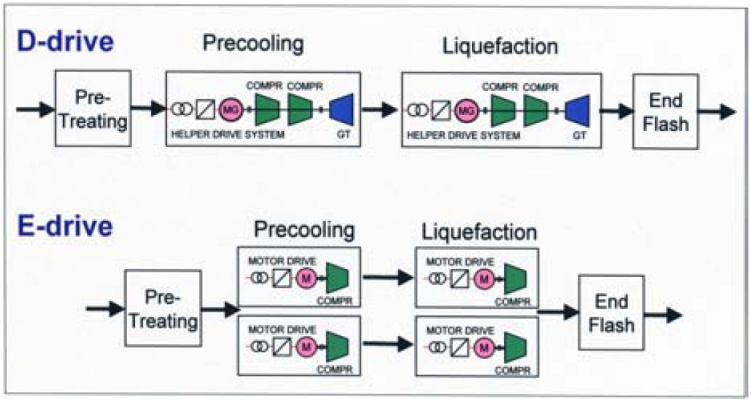

Figure 1.1.1: Direct- and Electric driven LNG liquifaction trains.

for electric motors. This means that switching to electric drivers takes the GTs off the project critical path. Switching to electric drivers thus reduces the project schedule risk by eliminating a schedule-driving event [1]. On the base case presented in Shu et. al. the Engineering Procurement and Construction (EPC) phase of the project was reduced by 2 months, translating into a life-cycle cost benefit of $125 million [1].

But as allways, there is no free lunch. Shu et. al. concludes that the switch to electric drivers will increase capital cost of investment, CAPEX, by approximately 5% and that the major adder is the large centralized power station [1]. However, both reduction of EPC schedule and increase in availability balances the increase in CAPEX, so that benefits are positive even if only one of them should be achieved [1].

1.1.2 Fixed speed Electric LNG

As noted in the above, Electric LNG (E-LNG) facilities should have a positive net present value even though it means a higher CAPEX as compared to the traditional direct drive concept. However, if variable speed is not critical to the cooling process, i.e. the LCIs are mainly used for starting the motors, or if process tuning could be done in another way, fixed speed compressor drives might be a reasonable alternative. Removing the LCIs and their respective isolating transformers could significantly reduce CAPEX. Fixed speed drives could also reduce operating costs, OPEX, by improving the thermal efficiency of electric system by removing them LCIs entirely. In addition, fixed speed drives would entail one less component to maintain and one less component that could fail.

In the general case, fixed speed Electric LNG looks favorable in cases where the facility is very large, i.e. 5-7 liquefaction trains. In this case some of the process trains may be of the fixed speed type, in effect constituting the base production of the facility, and the remaining trains being of variable speed type in order to tune the production to meet contract obligations.

If variable speed is required due to variations in the feed gas composition, an alternative

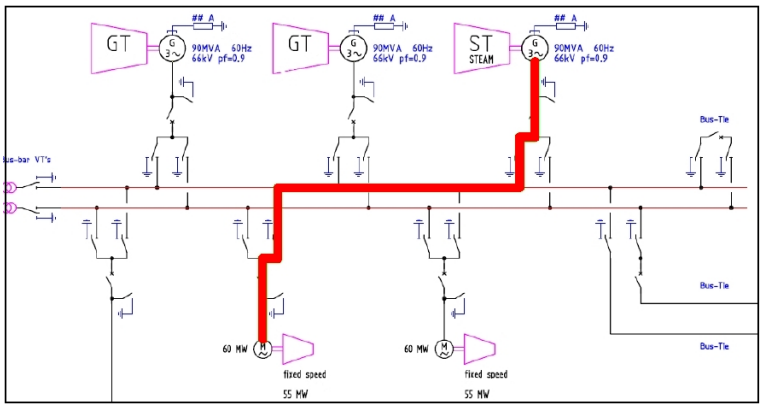

Figure 1.1.2: Dual bus-bar configuration.

could be to use variable speed drives on the first cooling steps and fixed speed on the last step, which would have a homogenous gas composition, i.e. pure methane. However, several problems arise concerning the feasibility of such a fixed speed solution. One of these problems is the manner of which to start the motors. In theory the cooling process could be parallelled as in figure 1.1.1 in infinity, decreasing the required power of the compressor at each step. However, this would make the process very expensive. In order to achieve some economy of scale, Kauffman et. al recommends the drivers to be as large as possible, for example 65 MW as delivered by Siemens. According to M. Kazi, the largest machine that could be started direct on line (DOL), assuming a 3% voltage dip requirement, would be approximately 6 MW at 132 kV [3]. It thus seems obvious that DOL starting of 65 MW machines is out of the question. In addition many of the other known starting methods, (such as reactor starting, auto-transformer starting, and solid state starters,) are unpractical because of the large thermal stresses these need to be rated for with starting currents at 4-5 pu [3].

It has been suggested that Motorformers should be applied as motors and generators for the fixed speed system. This is because they can be designed to operate at a very high voltage, e.g. 66 kV, and thus eliminate transformers. This would simplify starting by removing reactance and further compact the system.

It is thus the main objective of this thesis to investigate the feasibility of three alternative Back-to-Back starting methods available to the fixed speed concept. These are low frequency (synchronous) starting, partial frequency starting and soft starting. In addition, an inquiry will be made into the consquences of the fixed speed scheme to the grid. Starting simulations will be performed on shop model- and motorformer data, while dynamic grid simulations will be performed on Motorformer data only.

1.1.3 Starting methods

In order to facilitate the fixed speed starting concepts in question, a dual bus-bar system is required. This is in order to isolate one motor and one generator on a bus bar, while the other is operating at rated frequency supplying auxiliary systems and the operational

compressor drives. In this manner one generator and turbine can be used to start one motor and compressor set, accelerate it to rated frequency and synchronize with the other bus. Figure 1.1.2 shows a schematic of a dual bus-bar system with generators and motors. Using this kind of connection there are three suggested starting methods: Low frequency-, partial frequency, and soft starting.

Low frequency starting

Low frequency starting using a Back-to-Back configuration as explained in the above has been used for a long time. It has typically been used in starting of generators/motors in pumped storage hydro electric power plants, and has mostly been done for unloaded conditions [4], [5], [6]. Low frequency is also the starting method used when LCIs are employed.

The low frequency starting process is also called synchronous starting, and it is characterized by accelerating the generator and motor while synchronized. Because the motor now supplies its own reactive power the starting is pronouncedly gentle, with maximum starting currents limited to 150% - 200% of full load current [7].

The generator and motor are initially at stand still with their respective rotors magnetized. The starting process then begins by applying mechanical torque to the generator by the prime mover, i.e. any kind of turbine. The generator will then accelerate according to applied torque and friction breakaway torque, inducing voltages in its stator. These voltage will also appear in the motor and a current will start to flow, producing an electromagnetic torque in the motor as it interacts with the rotor field and the dampe windings. Hopefully the motor acheives breakaway and synchronizes with the generator after a few hunting cycles. From then on the generator and motor accelerates synchronously.

Partial frequency starting

Partial frequency starting is essentially the same as DOL-starting, except it takes place isolated from the remaining grid and at a lower frequency. The generator is run at a reduced speed, seperated from the motor by a breaker, with its rotor magnetized. The motor is at standstill without excitation. At a certain time the breaker is closed,

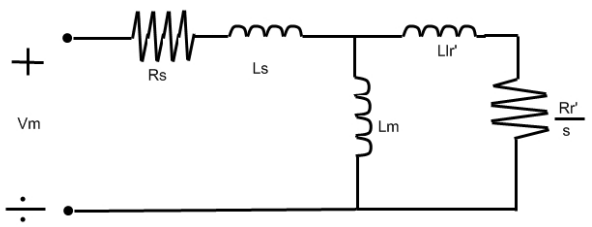

Figure 1.1.3: Basic equivalent cirucit of an induction machine.

currents are induced in the motor damper windings, field winding, and rotor surface. The motor is started as an induction machine to a reduced speed, where it is magnetized and synchronized with the generator.The reduced frequency is mainly due to:

1. According to basic induction machine theory, the initial in rush current to the motor will be dependant on the slip, s, i.e. the difference between motor speed synchronous speed, as shown in figure 1.1.3 [8].
2. When the motor accelerates, it brings the compressor up to speed with it. With a quadratic torque-speed curve for the compressor, reducing frequency means reducing the load at which synchronization is attempted quadratically.

Soft starting

This scheme uses the generator to emulate a soft starting device. The generator and motor is connected together in a Back-to-Back configuration, with the unmagnetized generator running at a reduced speed and motor at standstill. At a certain time, the generator magnetizing current is ramped up, gradually increasing the induced voltages in the stators of the respective machines. Referring to figure 1.1.3, the amplitude of the AC-voltage V_m is ramped up as the motor gains speed. Hence the starting currents and thermal loading of the damper windings is reduced. When the motor reaches a certain speed, its rotor is magnetized and it is synchronized with the generator as in the above.

1.2 Theory

In this section theory relevant to the work performed in the thesis will be presented. Emphasis has been put on basic synchronous machine theory because it helps build a foundation uppon which it is possible to perform and understand laboratory measurements and simulations. For a more specific litterature search on actual applications of Back-to-Back low frequency starting, general reference is made to the pre-project performed in autumn 2008 [9].

1.2.1 Flux linkages in synchronous machines

In synchronous machines, the stator self- and mutual inductances vary with the position of the rotor. Variations in inductances are caused by variations in the permeance of the magnetic flux path due to non-uniform air gap ([10], 59). Though most pronounced in salient pole machines, these variations will also be found in round rotor machines because of the large number of slots milled in the rotor to facilitate field windings ([10], 59). These variations are relevant because they are an imporant feature of the machine paramters. Variations in flux path permeance as a function of rotor position can be approximated as:

$$P = P_0 + P_2 \cos 2\varepsilon \tag{1.1}$$

where ε electrical is angle from the d-axis as shown in figure 1.2.1.

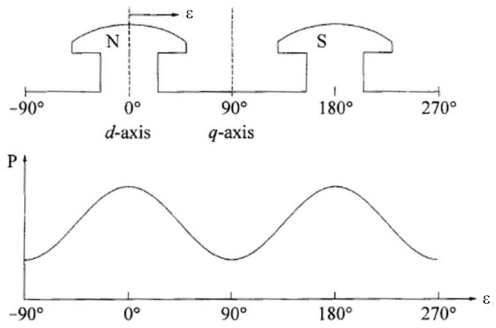

Figure 1.2.1: Variation of permeance with rotor position

Stator circuit equations

The three phase voltage equations for a synchronous machine are shown in 1.2, 1.3 and 1.4. Equation 1.5 shows the flux linkage in phase a, λ_a. The expressions for b- and c-phases are almost identical ([10], 61):

$$e_a = p\lambda_a - R_a i_a \tag{1.2}$$
$$e_b = p\lambda_b - R_a i_b \tag{1.3}$$
$$e_c = p\lambda_c - R_a i_c \tag{1.4}$$

$$\lambda_a = -l_{aa} i_a - l_{ab} i_b - l_{ac} i_c + l_{afd} i_{fd} + l_{akd} i_{kd} + l_{akq} i_{kq} \tag{1.5}$$

Stator self inductance

The a-phase self-inductance, l_{aa}, is defined as the ratio of the flux linking the a-phase winding to the phase current i_a, or: $l_{aa} = \frac{\lambda_{aa}}{ia}$, when all other currents are zero. It is directly proportional to the flux path permeance. According to equation 1.1 this permeance has a second harmonic variation. l_{aa} will be at a maximum every 180° at $\varepsilon = 0$, $\varepsilon = 180$ etc, and minimum at $\varepsilon = 90$, $\varepsilon = 270$ [10].

Neglecting space harmonics, the magnetomotive force (mmf) of phase-a may be resolved along the d- and q-axis accordingly:

$$\begin{aligned} MMF_{ad,peak} &= N_a i_a \cos\theta \\ MMF_{aq,peak} &= N_a i_a \cos((\theta + 90^\circ)) = -N_a i_a \sin\theta \end{aligned}$$

Here N_a is the effective number of turns in phase-a and θ as in figure 1.2.2.

This yields d- and q-axis fluxes

$$\begin{aligned} \Phi_{gad} &= (N_a i_a \cos\theta) P_d \\ \Phi_{gaq} &= (-N_a i_a \sin\theta) P_q \end{aligned}$$

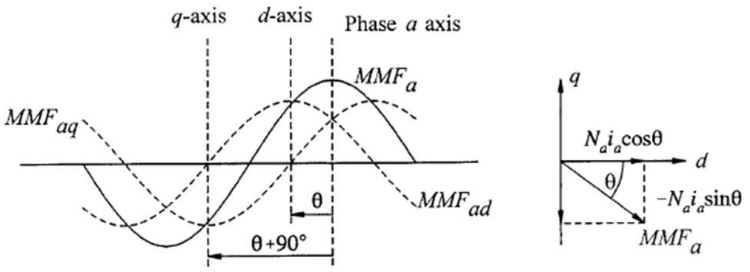

Figure 1.2.2: Phase-a mmf and its components.

and total air-gap flux linking phase-a:

$$\begin{aligned}\Phi_{gaa} &= \Phi_{gad}\cos\theta - \Phi_{gaq}\sin\theta \\ &= N_a i_a \left(P_d \cos^2\theta + P_q \sin^2\theta\right) \\ &= N_a i_a \left(\frac{P_d + P_q}{2} + \frac{P_d - P_q}{2}\cos 2\theta\right)\end{aligned}$$

From this, the phase-a self-inductance due to air-gap flux is ([10], 62):

$$l_{gaa} = \frac{N_a \Phi_{gaa}}{i_a} \tag{1.6}$$

$$= N_a^2 \left(\frac{P_d + P_q}{2} + \frac{P_d - P_q}{2}\cos 2\theta\right) \tag{1.7}$$

Adding leakage inductance, one obtaines total self-inductance for the a-phase ([10], 63).

$$\begin{aligned}l_{aa} &= L_{al} + l_{gaa} \\ &= L_{al} + L_{g0} + L_{aa2}\cos 2\theta \\ &= L_{aa0} + L_{aa2}\cos 2\theta\end{aligned}$$

and since the windings of phases-b and -c are assumed to be identical to those of phase-a and shifted 120°:

$$\begin{aligned}l_{bb} &= L_{aa0} + L_{aa2}\cos\left(2\theta - \frac{2\pi}{3}\right) \\ l_{cc} &= L_{aa0} + L_{aa2}\cos\left(2\theta + \frac{2\pi}{3}\right)\end{aligned}$$

The inductances can further be defined in the dq0 reference frame as ([10], 69):

$$L_d = L_{aa0} + L_{ab0} + \frac{3}{2}L_{aa2} \tag{1.8}$$

$$L_q = L_{aa0} + L_{ab0} - \frac{3}{2}L_{aa2} \tag{1.9}$$

$$L_0 = L_{aa0} - 2L_{ab0} \tag{1.10}$$

1.2.2 Three phase short circuit on synchronous machine

The behavior of a synchronous machine after short circuit gives valuable information about the construction of the machine. Hence it is an important part of the diagnostics-

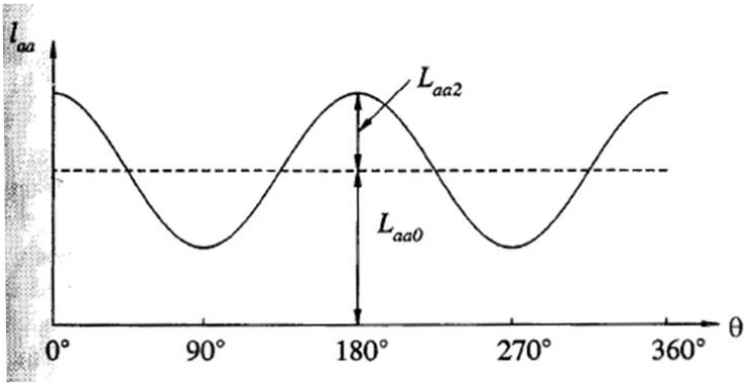

Figure 1.2.3: Phase-a self inductance variations.

and parameter estimation process. In the following the effects of a sudden three-phase short circuit on the terminals of an unloaded synchronous machine is presented. Also, the process of extracting parameters from the results is described.

After a sudden bolted three-phase fault, the resulting current consists of two distinct components. According to Kundur ([10], 109), these are:

1. A fundamental frequency component which initially decays very rapidly, i.e. in a few cycles, and then decays relatively slowly, i.e. in a matter of seconds.
2. A DC component which decays exponentially in several cycles.

The initial rapid decay of the AC component is due to the rapid decay of the flux linking the sub-transient circuits. That is, the current induced in the damper windings decay very fast. The AC component also has a slowly decaying component and this is due to the relatively slow decay of the flux linking the transient circuits, meaning that the current in the field winding or in the rotor iron surface decay relatively slowly ([10], 108).

Turning to the second part, the DC components have different magnitudes in the three phases, the sum of which is zero. They all decay with the armature time constant, T_a, which is equal to the ratio of the armature inductance to the armature resistance ([10], 108). Figure 1.2.4 illustrates the currents in the stator-, field- and damper windings following a symmetrical short circuit ([11], 101). It shows:

a) The DC component of the phase current resulting from the law of constant flux linkeages and its corresonding AC components in the field- and damper windings.

b) The AC component of the phase current and its corresponding DC components in the field- and damper winding.

c) The resulting currents in phase-, field-, and damper windings.

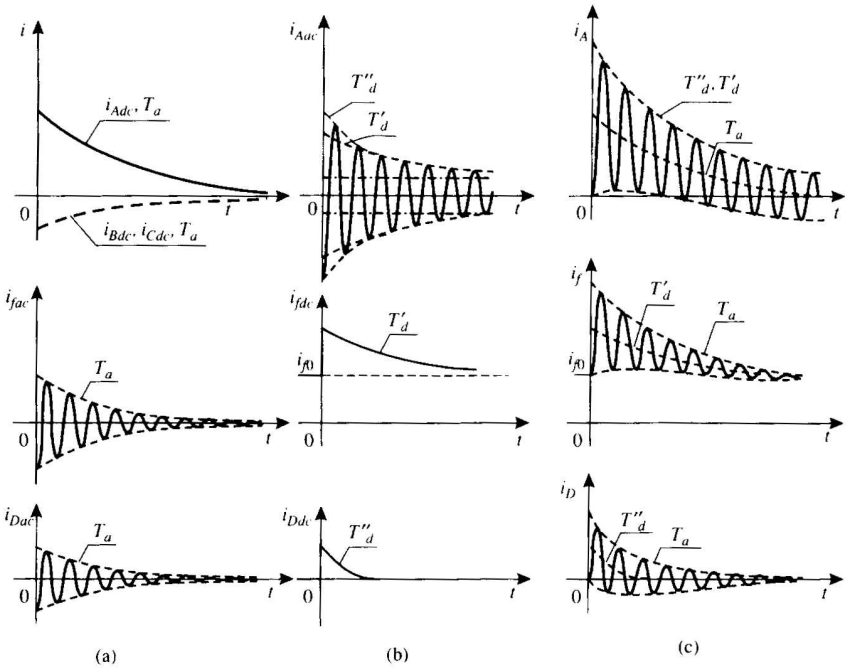

Figure 1.2.4: The various induced AC and DC currents in armature and rotor windings resulting from a sudden short-circuit

Parameter extraction

According to E. Mouini et. al. the resulting AC component of the stator current following a sudden three phase short circuit can be expressed as [12]:

$$i = V_m \left[\frac{1}{x_d} + \left(\frac{1}{x_d^{'}} - \frac{1}{x_d} \right) e^{-\frac{t}{T_d^{'}}} + \left(\frac{1}{x_d^{''}} - \frac{1}{x_d^{'}} \right) e^{-\frac{t}{T_d^{''}}} \right] \cos(\omega t + \theta_0) \tag{1.11}$$

The equation for the envelope is simply the expression within the brackets in equation 1.11:

$$i_{env} = V_m \left[\frac{1}{x_d} + \left(\frac{1}{x_d^{'}} - \frac{1}{x_d} \right) e^{-\frac{t}{T_d^{'}}} + \left(\frac{1}{x_d^{''}} - \frac{1}{x_d^{'}} \right) e^{-\frac{t}{T_d^{''}}} \right] \tag{1.12}$$

The steady state direct axis reactance may be found by considering equation 1.12 as the exponential terms have decreased to negligible values [12]:

$$x_d = \frac{V_m}{i_{steady}} \tag{1.13}$$

By subtracting the steady state current from equation 1.12 and assuming that $T_d^{'} \gg T_d^{''}$, we get an expression for the transient enveloping curve [12]:

$$i_{env} - i_{steady} \approx V_m \left[\frac{1}{x_d} + \left(\frac{1}{x_d^{'}} - \frac{1}{x_d} \right) e^{-\frac{t}{T_d^{'}}} \right] \tag{1.14}$$

The semi logarithmic method can be used as follows [12]:

$$\ln(i_{env} - i_{steady}) \approx At + B$$

Transient parameters are thus calculated:

$$T_d^{'} = -\frac{1}{A}$$
$$\ln\left(V_m\left(\frac{1}{x_d^{'}} - \frac{1}{x_d}\right)\right) = B$$

Likewise, subtracting the transient envelope and the steady state current from the original envelope, an expression for the sub-transient envelope is established [12]:

$$\ln(i_{env} - i_{steady} - i_{trans}) \approx A^{'}t + B^{'}$$

$$T_d^{''} = -\frac{1}{A^{'}}$$
$$\ln\left(V_m\left(\frac{1}{x_d^{''}} - \frac{1}{x_d^{'}}\right)\right) = B^{'}$$

1.2.3 Transferred power

In the following, the basic equations concerning power flow for machines will be developed. A very basic circuit consisting of two voltages and an impedance will form the basis for the derivation, which will end up at the power angle characteristics of a machine connected to a grid. Two synchronous machines connected Back-to-Back is in essence simply two voltages connected by an equivalent impedance, the following is thus of particular interest.

For a given circuit consisting of two AC voltages, $\hat{E_1}$ and $\hat{E_2}$, connected by an impedance Z with the current $\hat{I}$ flowing through the circuit from 1 to 2 as in figure 1.2.5 (a), the power at the load end will be [13]:

$$P_2 = E_2 I\cos(\phi_2) \tag{1.15}$$

In equation 1.15 ϕ_2 is the phase angle with respect to E_2. The phase current can be expressed as:

$$\hat{I} = \frac{\hat{E_1} - \hat{E_2}}{Z}$$

or:

$$\hat{I} = \frac{E_1\angle\delta - E_2\angle 0^\circ}{|Z|\angle\phi_z}$$
$$\hat{I} = \frac{E_1}{Z}\angle\delta - \beta z - \frac{E_2}{|Z|}\angle - \beta z \tag{1.16}$$

Where E_1 and E_2 are the magnitudes of the voltages $\hat{E_1}$ and $\hat{E_2}$ and δ is the angle between them as shown in figure 1.2.5 (b).

The real part of equation 1.16: is

$$I\cos(\phi_2) = \frac{E_1}{|Z|}\cos(\delta - \beta z) - \frac{E_2}{|Z|}\cos(-\beta z)$$

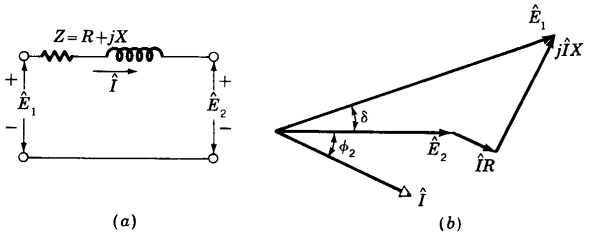

Figure 1.2.5: (a) Simple ac circuit with impedance. (b) Corresponding phasor diagram.

By noting that

$$\cos(-\beta z) = \cos(\beta z) = \frac{R}{|Z|}$$

we see that substitution into equation 1.15 gives:

$$\begin{aligned} P_2 &= \frac{E_1 E_2}{|Z|}\cos(\delta - \beta z) - \frac{E_2^2 R}{|Z|^2} \\ &= \frac{E_1 E_2}{|Z|}\sin(\delta + \beta_z) - \frac{E_2^2 R}{|Z|^2} \end{aligned} \tag{1.17}$$

We know that torque can be expressed as:

$$T_2 = \frac{P_2}{\omega_2}$$

Giving:

$$T_2 = \frac{1}{\omega_2}\left[\frac{E_1 E_2}{|Z|}\sin(\delta + \kappa_z) - \frac{E_2^2 R}{|Z|^2}\right] \tag{1.18}$$

Similarly:

$$P_1 = \frac{E_1 E_2}{|Z|}\sin(\delta - \alpha_z) + \frac{E_1^2 R}{|Z|^2} \tag{1.19}$$

where $\kappa_z = 90° - \beta_z = \tan^{-1}(\frac{R}{X})$.

If resistance is negligible, then $\kappa_z \approx 0$ and we get:

$$P_1 = P_2 = \frac{E_1 E_2}{X}\sin(\delta)$$

Similarly, the received reactive power is:

$$Q_2 = E_2 I \sin(\phi_2) \tag{1.20}$$

and the imaginary part of 1.16 is:

$$I\sin(\phi_2) = \frac{E_1}{|Z|}\sin(\delta - \phi_z) - \frac{E_2}{|Z|}\sin(-\beta_z)$$

Moreover:

$$-\sin(-\beta_z) = \sin(\beta_z) = \frac{X}{|Z|}$$

Again, substituting into equation 1.20 gives:

$$Q_2 = \frac{E_1 E_2}{|Z|}\sin(\delta - \beta_z) + \frac{E_2^2 X}{|Z|^2} \tag{1.21}$$

$$= \frac{E_1 E_2}{|Z|}\cos(\delta + \kappa_z) + \frac{E_2^2 X}{|Z|^2} \tag{1.22}$$

and

$$Q_1 = \frac{E_1 E_2}{|Z|}\cos(\delta - \kappa_z) - \frac{E_2^2 X}{|Z|^2} \tag{1.23}$$

1.2.4 $\frac{d\Delta Q}{dV}$ - criterion for voltage stability

Due to the laboratory experiments being conducted with a relatively large inductor in operation, the dynamics of voltage stability is of concern. In the following one of many criterions which have been formulated on voltage stability will be presented.

The $\frac{d\Delta Q}{dV}$ - criterion is based on the capability to supply the load with reactive power for a given real power. Assuming that resistance is negligible and that the load is dependant on voltage, equations 1.19 and 1.23 becomes ([11], 240):

$$P_1(E_2) = \frac{E_1 E_2}{X}\sin(\delta) = P_2(E_2) \tag{1.24}$$

$$Q_1(E_2) = \frac{E_1 E_2}{X}\cos(\delta) - \frac{E_2^2}{X} \tag{1.25}$$

Using the trigonometric identity $\sin^2(\delta) + \cos^2(\delta) = 1$, the apparent power is expressed ([11], 241):

$$\left(\frac{E_1 E_2}{X}\right)^2 = P_2^2(E_2) + \left[Q_1(E_2) + \frac{E_2^2}{X}\right]^2$$

And by solving for $Q_1(E_2)$ we obtain:

$$Q_2(E_2) = \sqrt{\left[\frac{E_1 E_2}{X}\right]^2 - [P_2(E_2)]^2} - \frac{E_2^2}{X} \tag{1.26}$$

Equation 1.26 gives the reactive power-voltage characteristic and treats the load voltage E_2 as variable. For a stiff active load which is not dependant on voltage, equation 1.26 has a parabolic shape as shown in figure 1.2.6. It also shows the effect of increasing load power P_2, i.e. shifting the curve downwards and to the right ([11], 241).

As can be seen in figure 1.2.6, $Q_1(E_2)$ crosses the horizontal axis in $E_2 = E_1$ for $P_2 = 0$, and peaks at $E_2 = \frac{E_2}{2}$ for a maximum value of $Q_1(\frac{E_2}{2}) = \frac{E_1^2}{4X}$. For $P_2 > 0$ $Q_{1,max}$ occurs at

$$E_2 = \sqrt{\left[\frac{E_1}{2}\right]^2 + \left[\frac{P_2(E_2)X}{E_1}\right]^2}$$

which is greater than $\frac{E_1}{2}$ ([11], 241).

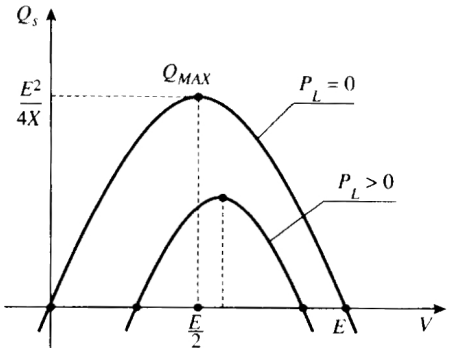

Figure 1.2.6: $Q_1(E_2)/Q_S(V)$ characteristic. $P_2 = 0$ and $P_2 > 0$

If one superposes the reactive power characteristic of the load, as in figure 1.2.7, one may observe two equilibrium points. These are marked as u and s in figure 1.2.7([11], 242).

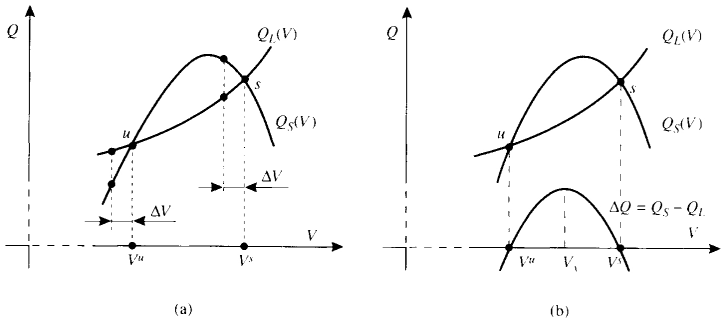

Figure 1.2.7: Demanded and supplied reactive power as function of load voltage E_2/V

It can be seen that in equilibrium point s, an incremental decrease in E_2, or V, leads to an increase in supplied reactive power, Q_1/Q_S and a decrease in load reactive power, Q_2/Q_L. While at point u, the situation is opposite: An incremental decrease in load voltage E_2/V leads to a decrease in supplied reactive power Q_1/Q_S. It is thus evident that point s is a stable operating point because it leads to a surplus in reactive power that restores the voltage, while point u is unstable because a cascading voltage collapse will ensue an incremental decrease ΔE_2. Formalized ([11], 242):

$$\frac{d(Q_S - Q_L)}{dV} < 0$$

Chapter 2

Experimental work

In the following an account will be made on the experimental work conducted during the course of the masters thesis. The laboratory experimental setup will be described together with the process of parameter estimation and the starting experiments. The experiments were conducted in the synchronous machine laboratory at NTNU. The machines are normally used for educational purposes, i.e. basic synchronous machine- and magnetic field exercises. The synchronous machines are mounted on a common shaft with a DC machine, which for our purposes will act as turbine and compressor respectively.

The main purpose of these experiments is to verify the simulation model presented in section 3.2 and, if possible, to identify practical challenges that are not evident in a simulation model. The setup from the laboratory will be replicated in the simulation model and the respective results compared. This chapter will present the experimental setup and the experimental results.

2.1 Experimental setup

A synchronous machine laboratory workstation comprises one synchronous machine and one DC-machine mounted on a common shaft. The DC-machine is controlled by a Siemens SIMOREG motor drive. Figure 2.1.2 shows a schematic of the DC-motor drive while figure 2.1.3 shows a schematic of the synchronous machine workstation circuit.

The synchronous machines may be connected to the 230 V grid or to a bus featuring a short circuit contactor, a water cooled resistor bank and an open outtake labelled 4, 5 and 6 in figure 2.1.3. The outtake is meant for connecting capacitive or inductive loads. Using these open ports the generator and motor stators were connected together via a variable inductance and a switched contactor. The Back-to-Back mounting scheme is shown in figure 2.1.4.

The instrumentation on the DC-motor drives were largely analogue ± 10 volt signals. It was thus convenient to leave control of the DC-machines to the already existing motor

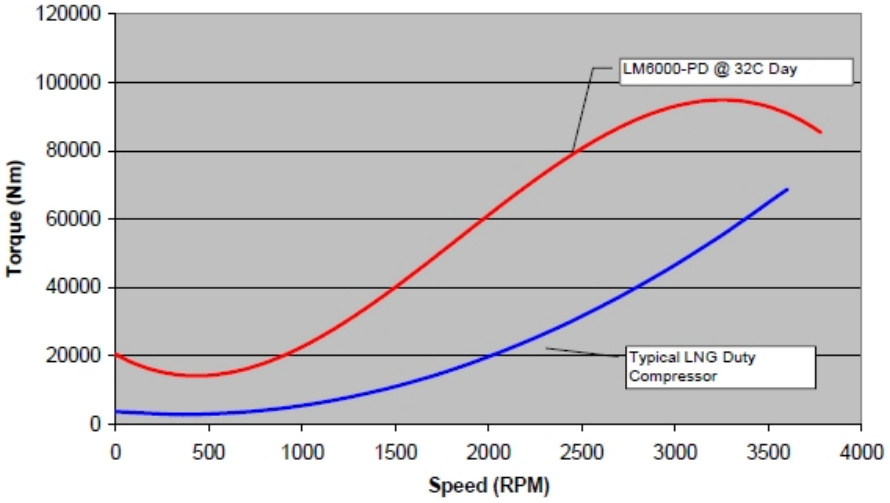

Figure 2.1.1: Typical GE LM6000 and Compressor torque-speed characteristics

drive, while the speed and armature current could be processed in Labview. A PCI card with multiple analogue ports was acquired for the purpose of interfacing the SIMOREG and Labview.

The goal was to control the DC-machines so as to recreate curves shown in figure 2.1.1, taken from [14] and thus emulate the turbine and compressor. The plot of the gas turbine characteristic was made by selecting points on the turbine curve in figure 2.1.1 manually, and fitting these to a fourth order polynomial using Curve Expert version 4.5. As for the compressor characteristic, a plot was made from a torque-speed characteristic of a typical LNG sub-cooling compressor with 12 data points. This gave:

$$T_t(n) = 20274.5 - 20.75 \cdot n + 0.02605 \cdot n^2 - 1.01785e^{-6} \cdot n^3 - 8.9908e^{-6} \cdot n^4 \quad (2.1)$$

$$T_c(n) = 2999.9998 - 4.5329319 \cdot n + 0.012591478 \cdot n^2 \quad (2.2)$$

Where T_t and T_c is turbine- and compressor torque respectively, and n is the speed in rpm.

For the turbine, the per unit base value was chosen so as to produce 0.8 pu torque at rated speed, i.e. 3600 rpm. This was done due to the bump in characteristic towards the end of the speed range. If the output had been 1 pu at 3600 rpm, the bump would bring the output beyond the 10 V limit set by the PCI card interfacing Labview and the motor drive. Thus:

$$T_{base,t} = 105853$$
$$T_{base,c} = 149867$$

For the keen observer it is immediately obvious that the compressor is more powerful than the turbine. This is because the compressor is rated at 56.6 MW while the LM6000

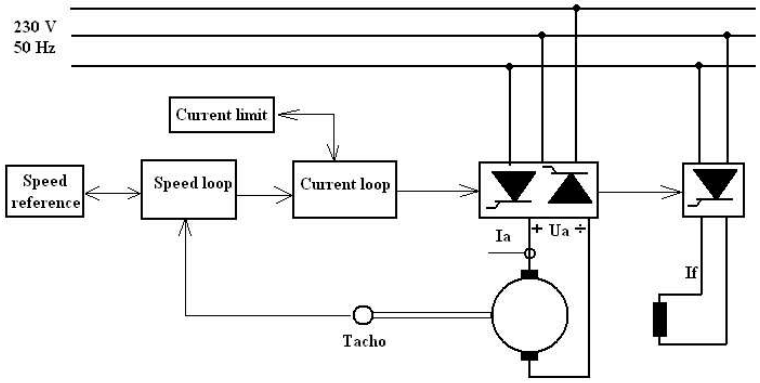

Figure 2.1.2: Schematic of DC-motordrive.

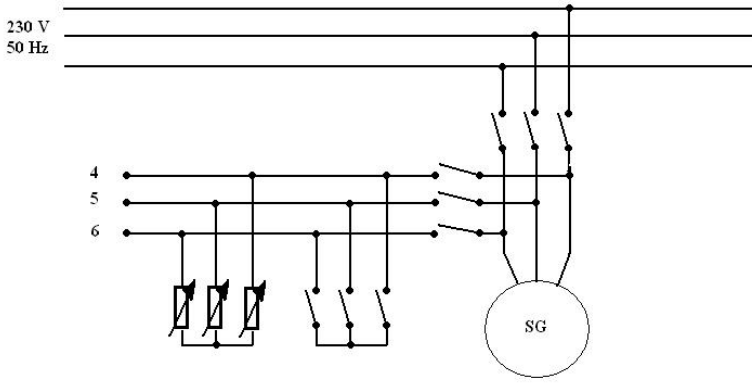

Figure 2.1.3: Synchronous machine laboratory workstation circuit.

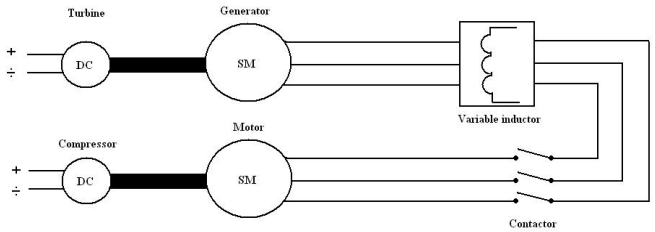

Figure 2.1.4: Synchronous machines connected Back-to-Back with common shaft DC-machines.

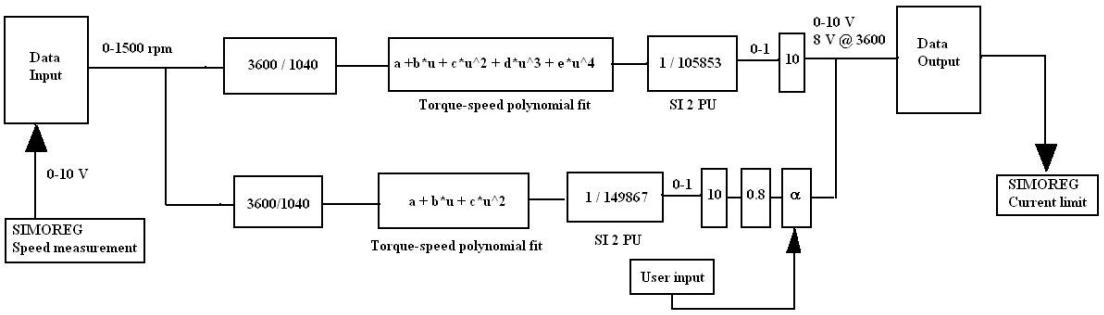

Figure 2.1.5: Block diagram of labview torque control program.

in question yields a mere 32.5 MW. The particular turbine has been chosen because it has a verifiable torque-speed characteristic for the entire speed range. For our purposes the turbine has been scaled, which might be sub-optimal but noting that primer movers is not the focus of this thesis, it does not render the electric feasibility study invalid. The availability of higher power turbines and their ability to produce torque at low speeds will be discussed later in section 3.3.

Labview uses equations 2.1 and 2.2 to calculate the DC-machine current limit as a function of the measured speed. Speed reference could then be set on the workstation desk, and upon issuing the start command the turbine machine would accelerate while injecting only as much current as is given by equation 2.1 for that particular speed. The same applies to the compressor machine: The compressor speed reference was manually set to zero and the current limit controlled as a function of speed given by equation 2.2

A side effect of leaving speed control to the DC-motor drive was that the drive entered field weakening mode at approximately 1040 rpm. Field weakening introduces a non-linearity between injected current and produced torque([8], 7-19). It was therefore decided to use 1040 rpm as the system maximum speed. As can be seen in figure 2.1.5, the input to the torque-speed equations are appropriately corrected in order to ensure that the machines pass through the entire range. In effect, the torque-speed characteristics are compressed to fit in the 0-1040 range. Thus the simplification should not be detrimental to the results.

A compressor power control function was implemented simply by multiplying the current limit output for the compressor machine by a factor, α, ranging between 0-1. Effectively this means that at α=1, the compressor machine applies the same torque as the turbine at rated speed i.e. the turbine and the compressor are equally rated.

By input to the analogue card, it was possible to log the machine speeds and the armature currents of the DC-machines in addition to the calculated output values. The field currents were logged in a synthesized manner by logging the output of a simple function that gave the field current as a function of the applied command signal output from Labview. The functions were found experimentally and are:

$$I_{f,g} = 2.27x - 0.77 \tag{2.3}$$

$$I_{f,m} = x \tag{2.4}$$

where x is the output signal from Labview.

2.2 Parameter estimation

The synchronous machines in the laboratory setup are originally from 1946 and documentation is very scarce. In order to be able to recreate the setup in the laboratory as accurately as possible, extensive parameter estimation procedures were performed. In the following the results from the parameter estimation process is presented along with possible sources of error, assumptions, and simplifications.

2.2.1 Reactance measurements

In order to determine d- and q-axis reactances, a variable AC voltage source was, in the case of the star connected motor, connected between one of the stator terminals and the star point accessible in the junction box. In the case of the delta connected generator, all terminals in the junction box were isolated from each other. The AC voltage source was then connected to one of the phase terminals and the only other terminal that would produce a current, ensuring that the current only passed through one stator winding. Multimeters were used to measure the current flowing between the two connections as well as the voltage across them. At a certain voltage level the machine rotor was turned manually until the approximate maximum current was found. The current and voltage was then noted and the rotor was again turned by hand in order to find the minimum current position. In addition, the resistance of stator winding was measured by means of milliohm-meter. The results are rendered in table 2.2.1.

Machine	Voltage	Current
Generator high	10.35 V	6.56 A
Generator low	14.93 V	2.63 A
Motor high	7.94 V	5.69 A
Motor low	8.58 V	3.90 A

$$R_g = 0.31$$
$$R_m = 0.125$$

In the above it is assumed that measurement equipment is accurate. High quality Fluke multimeters were used for the reactance measurements and a high resolution resistance measurement brigde was used for the resistance measurements. However, inherent inaccuracy is associated with turning the rotor by hand and finding the minimum and maximum currents. This has been regarded as the biggest potential source of error to these reactance measurements.

Phase quantities

The above yields the following phase impedances:

$$Z_{g,min} = 1.57 \quad Z_{m,min} = 1.395$$
$$Z_{g,max} = 5.67 \quad Z_{m,max} = 2.2$$

By subtracting resistance we get the phase reactances.

$$\begin{aligned} X_{g,min} &= \sqrt{|Z_{g,min}|^2 - R_g^2} \\ X_{g,min} &= 1.539 \\ X_{g,max} &= 5.66 \\ X_{m,min} &= 1.389 \\ X_{m,max} &= 2.196 \end{aligned}$$

d- and q-axis quantaties

X_d and X_q, being proportional to L_d and L_q, can be calculated from equations 1.9 and 1.10. Using the approximation ([10], 65), $L_{ab0} \approx \frac{1}{2}L_{aa0}$, it follows that

$$L_d = L_{aa0} + L_{ab0} + \frac{3}{2}L_{aa2} = \frac{3}{2}L_{max}$$
$$L_q = L_{aa0} + L_{ab0} - \frac{3}{2}L_{aa2} = \frac{3}{2}L_{min}$$

and

$$\begin{aligned} X_d &= \frac{3}{2}X_{max} \\ X_q &= \frac{3}{2}X_{min} \end{aligned}$$

Thus the generator and motor reactances are:

	Generator	Motor
X_d	8.49	3.294
X_q	2.308	2.083

Table 2.2.1: Steady state d- and q-axis reactances.

2.2.2 Three phase short circuit test

In order to determine the machine time constants, a sudden short circuit test was performed on the machines. The machines where run at rated speed and excited to produce a reduced voltage so as not to cause damage to the windings. Current measurement

equipment was applied to one of the stator phases and to the field current supply. These outputs where fed to an oscilloscope that was set to be trigged as stator current started to flow. The data could then be downloaded to a laptop via Open Choice Desktop software.

Time constant estimation

The data was imported to Matlab where it could be manipulated and plotted. After plotting the stator phase current response, the peak value data points were selected manually and stored. From this data exponential curves could be fitted using CurveExpert.

Subtracting the steady state value, one curve was fitted from data points starting after the three first cycles. This was the transient enveloping curve. Then, subtracting steady state and the function value of the transient enveloping curve, a curve was fitted using data points from the peaks of the three first cycles after short circuit. All according to the procedure described in sub-section 1.2.2. The resulting exponential functions are:

	Transient	Sub-transient
Generator	$i_{env} = 55.52e^{-0.0068t}$	$i_{env} = 36.57e^{-0.0556t}$
Motor	$i_{env} = 30.56e^{-0.0066t}$	$i_{env} = 26.6e^{-0.0733}$

Table 2.2.2: Exponential fit of peak values for time constant estimation.

Figures 2.2.1 and 2.2.2 show the plots of the stator short circuit response along with the field current response. Superposed are plots of the exponential functions in table 2.2.2. It can be seen that the plots are fairly accurate and as can be seen in figure 1.2.4 (b), it is in accordance with the theory on the subject.

It should be noted that the field current has been filtered by a running average over ten data points, resulting in a time delay and peak damping. This is because the original data was very noisy due to the switching of the controlled DC current source. The field current waveform has also been amplified ten times to better comply with axes.

Close inspection of the negative peaks in the first few cycles in figures 2.2.1 and 2.2.2, gives evidence that the waveform contains a transient DC-term. This term is the transformed effect of the AC-term in the field winding current waveform as explained in sub-section 1.2.2. Although obviously present, efforts to filter out this term in order to obtain more precise sub-transient values were deemed excessively cumbersome. Table 2.2.3 shows the transient and sub-transient time constants in millisconds for the synchronous machines as calculated in the above. They are deemed sufficiently accurate for our purposes.

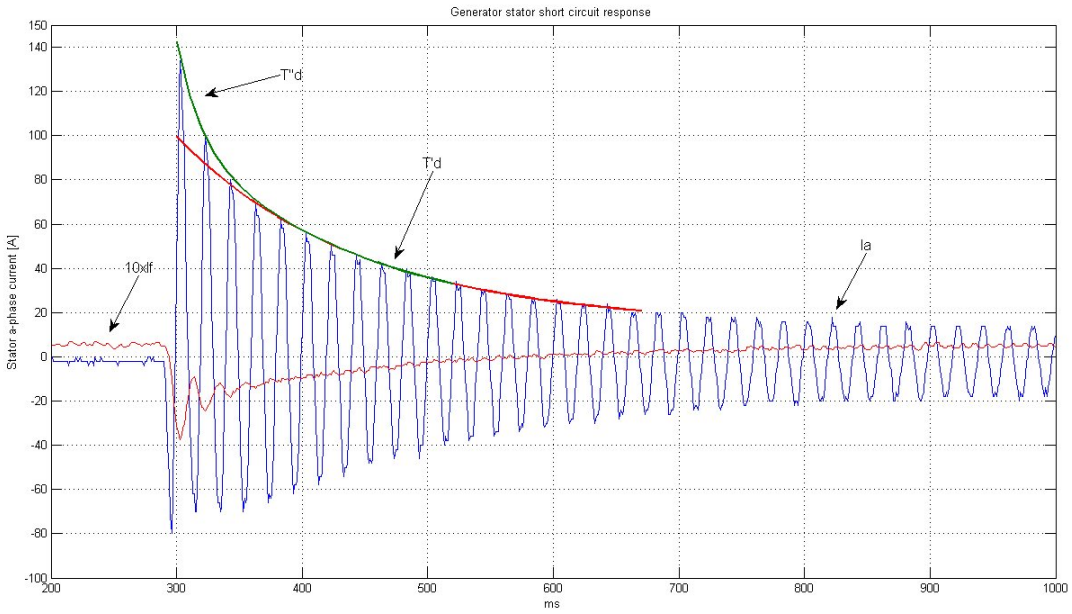

Figure 2.2.1: Generator short circuit response with superposed transient- and sub-transient enveloping curves.

	Generator	Motor
T'_d	146.64	150.62
$T''d$	17.96	13.96

Table 2.2.3: Generator- and motor time constants in milliseconds.

Transient and subtransient reactance estimation

Using the relations presented in section 1.2.2, the d-axis steady state-, transient-, and sub-transient reactances could be calculated. In order to determine q-axis reactances, steady state values had already been estimated using another procedure in section 2.2.1. However, the recalculations of the steady state quantaties may serve as a control. Being delta-connected, some transformations were done to the generator values:

$$X_{d,Y} = \frac{V_{m,ll}}{\sqrt{3} I_{ph}}$$

$$X_{\Delta} = 3X_Y$$

$$X_{d,\Delta} = \frac{\sqrt{3} V_{m,ll}}{I_{ph}}$$

It can be seen that the steady state values in table 2.2.4 are fairly similar to those calculated in section 2.2.1 and rendered in table 2.2.1. According to Mouni et. al. the quadrature axis parameters may be determined by application of Park's transformation on the currents after a short circuit [12]. However, this is beyond the scope of this thesis, and the following assumptions are made:

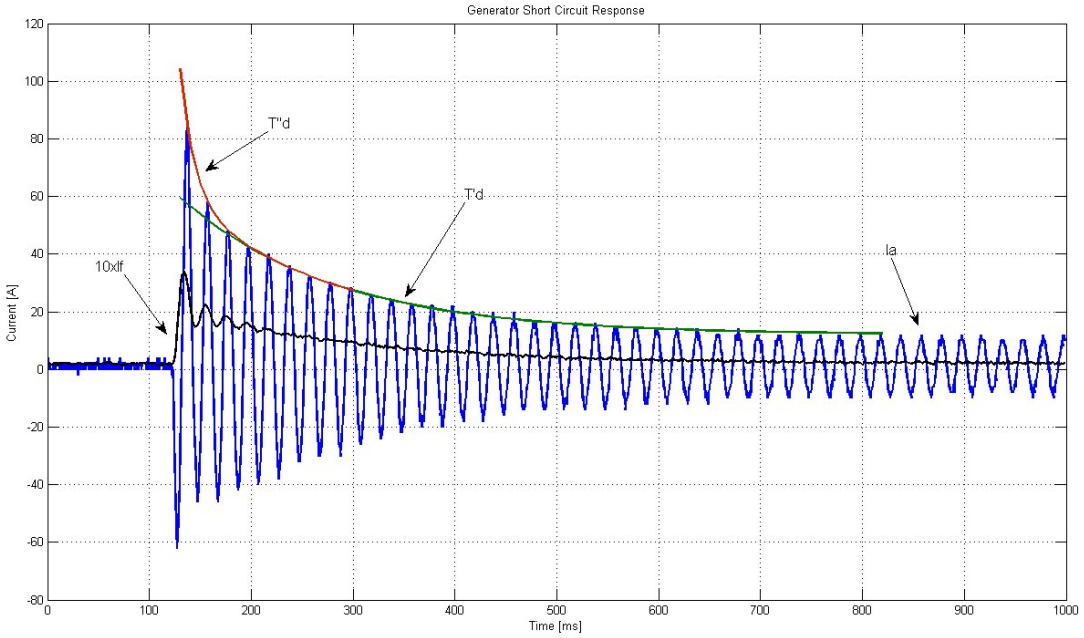

Figure 2.2.2: Motor short circuit response with superposed transient- and sub-transient enveloping curves.

	Generator	Motor
X_d	9.01	3.24
$X_d^{'}$	1.93	0.91
$X_d^{''}$	1.23	0.56

Table 2.2.4: D-axis reactances from short circuit tests.

1. The machine rotors are laminated, hence there is little or no screening in the q-axis in the transient state.
2. There is sub-transient saliency, i.e. There is considerable more damping in the d-axis than in the q-axis.

It thus follows from assumption 1 that $X_q^{'} = X_q$. From assumption 2, it follows that $X_q^{''} > X_d^{''}$ ([11], 105). At the same time it is reasonable to expect that even though there are no damper windings, other parts of the rotor iron and -copper opposes the rapidly changing fluxes by means of circulating currents, i.e. $X_q^{''} < X_q^{'}$, or: The q-axis

$$\begin{array}{ll} \text{Generator} & 1.23 < X_q^{''} < 2.3 \\ \text{Motor} & 0.56 < X_q^{''} < 2.08 \end{array}$$

sub-transient reactances are chosen at the middle point between its boundaries:

As previously mentioned, the transient DC-term in the short circuit response has been omitted. If it had been taken into account, the sub-transient time constants would have been somewhat larger. This is because, both in the case of the motor and the generator,

$$X''_{q,gen} = 1.76 \quad X''_{q,mot} = 1.32$$

the transient DC-term is positive. The points from which the exponential plots have been fitted, where also extracted from the positive side of the current plot. This means that some of the decline registered in the first few cycles is due to the armature time constant T_a and not the sub-transient time constant. The assumptions made regarding q-axis reactances are also a potential source of error.

2.2.3 Inertia estimation

The machine inertias were estimated by accelerating the unloaded generator while metering speed and turbine current. By choosing a segment during which the acceleration was linear, and hence the current fairly constant, the total inertia of the turbine-generator set could be calculated.

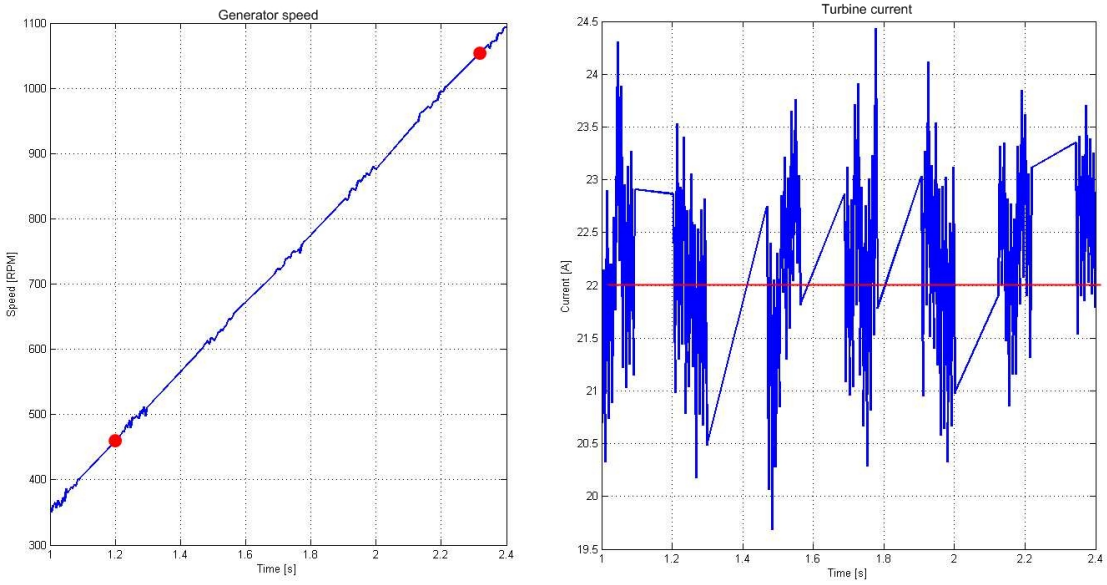

Figure 2.2.3: Linear acceleration and applied driving current.

Figure 2.2.3 shows the linear acceleration of the generator (left) and the turbine macine armature current (right). The points on the speed curve that was used have been marked, along with the approximate mean turbine current. They are:

(1.203s, 459.7 rpm) and (2.348s, 1061.5 rpm)
$I_{t,dc} \approx 22$ A

This gives:

$$\frac{\Delta\omega}{\Delta t} = 54.97 \tag{2.5}$$

$$T = k_T I_{t,dc} = 40.7Nm \tag{2.6}$$

$$=> J = \frac{T}{\dot{\omega}} = 0.74 \tag{2.7}$$

$$H = \frac{0.5J\omega_s^2}{S_n} \tag{2.8}$$

$$H = 0.506 \tag{2.9}$$

In the above, $k_T = 1.85$ is used. The estimation of k_T is shown in sub-section 2.2.7.

The greatest sources of error in estimating the inertia in this manner is the reading of the current to the right in figure 2.2.3 and the fact that friction and windage has been omitted. However, if these terms had been very strongly present in the above. The fact that these increase with speed would have cause the acceleration to the left in figure 2.2.3 flatten as speed increased. Hence, the fact that the acceleration linear lends credit to the approximations. The inertia estimation was performed on the generator machine, assuming that the results also applies to the motor. The motors are very similar in making, and their dimensions appear identical. Thus this simplication should not be detrimental to the credibility of the results.

2.2.4 Friction and windage

Bearing friction was estimated by running the turbine-generator set at different speeds while recording the input DC-motor current and speed. In this manner the mechanical torque could be calculated. However, due to the non-linearity as the DC-machine goes into field weakening, the friction torque needed to be plotted as a function of speed in the range 0-1000 rpm, and calculated for 1500 rpm. The results were:

I_{dc}	N
1.1	307
1.23	480
1.3	697
1.35	826
1.4	959

Table 2.2.5: Friction estimation.

From table 2.2.5 a linear plot was made in Curve Expert. It gave:

$$I_{dc}(n) = 4.38 \cdot 10^{-4} n + 0.989$$

$$I_{dc}(1500) = 1.647$$

$$T_{mech,f}(1500) = 3.04$$

$$T_{mech,fpu} = 0.026$$

There is always an uncertainty associated with extrapolating curves. In addition the curve fit is linear, effectively omitting the quadratic nature of the windage term. The test was performed with an unexited rotor, thus loss associated with eddy currents is neglected. As in the above, the test was performed on the generator, assuming the motor to be identical.

2.2.5 Open circuit characteristic

An open circuit test was performed on both machines in order to produce their respecive saturation characteristics. The machines were run at 1500 rpm, logging the terminal voltage as a function of applied field current. The characteristics are shown in figure 2.2.4 and the rated voltage and the corresponding field current have been marked. They are:

$$I_{f,rated,gen} = 1.56A \quad I_{f,rated,mot} = 1.08A$$

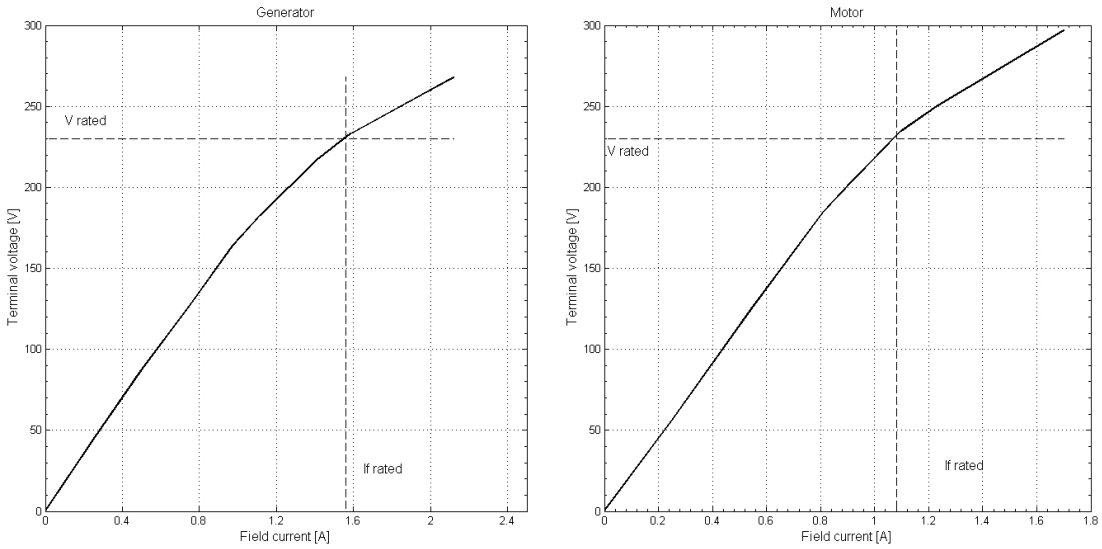

Figure 2.2.4: Generator- and motor open circuit characteristics.

With the possible exception of reading noisy field current measurements, there is little or no uncertainty associated with the open circuit measurements.

2.2.6 Inductor measurement

One of the sub-objectives of the thesis was to establish how inductance between the generator and motor affected starting. A large 5-step three-phase iron core inductor was used. It consisted of three legs, around which the coils was wound, mounted on an iron base. At the top there was also a round iron dish. The airgap between this dish and the legs could be varied by turning a crank handle. Unfortunately, during operation it was discovered that the airgap was asymmetrical. This meant that as current levels reached

a certain point the inductor would make a lot of noise and shake violently. Thus, it was necessary to even out the airgap with sheets of paper, which also meant that it could not be run at with the airgap fully closed.

In order to determine the inductance at each step, the generator was set to feed a resistive load through the inductor, measuring the voltage drop across- and the current through the inductor. The results are presented in table 2.2.6.

Level	Δ U	I_{ph}	f	X	L_{tot}	L_{step}
1	4.8	6.4	35	0.75	3.4	3.4
1	8.45	11.3	34.66	0.74	3.4	3.4
1	12.5	17.4	34.8	0.71	3.2	3.2
2	18.9	6.52	35	2.89	13.2	6.6
2	28.5	10.30	34.75	2.77	12.6	6.34
2	44	17.9	34.5	2.45	11.3	5.6
3	38.2	6.35	34.6	6.01	27.6	9.2
3	60.4	11.3	33.8	5.34	25.2	8.3
3	82.3	17.4	34.9	4.73	21.5	7.2
4	59.4	6.35	34.4	9.33	43.2	10.8
4	97.8	11.1	34.6	8.81	40.5	10.1
4	114	14	34.8	8.14	37.2	9.3

Table 2.2.6: Inductor parameters at steps 1-4

By observing L_{step} for the different steps, it is evident that there is a non-linearity in the inductance as a function of steps. This is due to the airgap not being closed, because as the number of turns increase, the same current gives a higher NI to cross the airgap and link with the top iron disk and the other legs.

2.2.7 DC motor parameters and Back-to-Back efficiency measurements

The estimation of DC motor parameters is crucial in order to describe the system and the measurement of efficiencies is necessary in order to gain an overview of the system. The efficiencies puts the results in section 2.3 into a larger context, in which it can be discussed.

The DC-machines are rated 7.9 kW for 44 A, and the armature resistance was measured to be approximately 0.8Ω by a multimeter. The turbine machine current limiter was set to maximum and the generator was coupled to the water cooled resistors. While keeping excitation and load resistance constant, the generator was run at increasing speeds while metering DC armature voltage and -current, line-to-line voltage, and phase current. In this manner it was possible to calculate the efficiencies of the DC-motor and the Synchronous Generator as well as the DC-motor torque constant k_T given by the

following relations:

$$\begin{aligned} P_{el} &= U_a I_a \\ E_a &= U_a - R_a I_a \\ P_{mech} &= E_a I_a \\ T_{mech} &= \frac{P_{mech}}{\frac{2\pi}{60} N_{rpm}} \\ P_{load} &= \sqrt{3} U_{l-l} I_{ph} \end{aligned}$$

And by definition we have:

$$\begin{aligned} \eta_{dc} &= \frac{P_{mech}}{P_{el}} \\ \eta_{gen} &= \frac{P_{load}}{P_{mech}} \\ k_T &= \frac{T_{mech}}{I_a} \end{aligned}$$

N	U_a	I_a	P_{el}	U_{l-l}	I_{ph}	P_{load}
200	44.4	7.1	315.2	35	1.9	118
405	88.3	12.0	1060.2	69	5.1	620
602	130.1	16.5	2146.6	103	8.2	1463
802	172.1	20.7	3562.5	136	11.1	2614
902	192.7	23.1	4451.3	151	12.5	3269
1115	230.0	28.4	6532.0	186	15.5	4993
1291	234.0	36.7	8587.8	214	17.7	6530

Table 2.2.7: Efficiency measurement results.

N	η_{dc}	η_{gen}	k_T	P_{load}
200	0.87	0.43	1.849	118
405	0.89	0.65	1.857	620
602	0.89	0.75	1.855	1463
802	0.90	0.81	1.853	2614
902	0.90	0.81	1.845	3269
1115	0.90	0.84	1.776	4993
1291	0.87	0.87	1.514	6530

Table 2.2.8: Calculated efficiencies and torque constants.

The results are shown in table 2.2.7 and the calculated η, k_T and P_{load} are shown in table 2.2.8. Not surprisingly the machine efficiencies increase as speed and thus loading increases. It is evident that the increase is especially pronounced in the synchronous machine. This is to be expected as the machine rating of 18 kVA is relatively high compared to that of the driving DC-machine. One may also observe in table 2.2.8 that the torque constant dip as the DC-motor drive goes into field weakening at approximately 1040 rpm.

An efficiency measurement on the entire system when connected Back-to-Back was also conducted. With the generator and motor connected together, the turbine machine

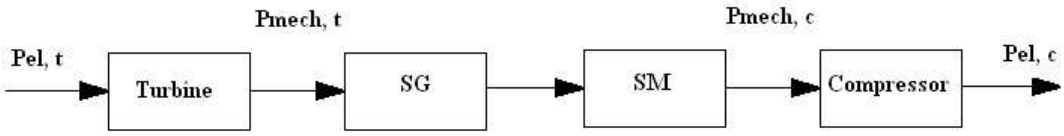

Figure 2.2.5: Power balance illustration.

current limiter was manually set to maximum and the system was run at different speeds while loading was varied by manipulating the compressor machine current limit.

N	$U_{a,t}$	$I_{a,t}$	$U_{a,c}$	$I_{a,c}$	η_{tot}
300	67.7	12.6	54.0	6.5	0.41
304	80.5	32.1	45.0	21.0	0.37
605	127.8	11.6	115.5	5.9	0.46
603	136.0	27.6	105.0	19.7	0.55
908	188.6	12.3	175.5	6.2	0.47
912	196.6	27.1	166.1	19.6	0.61
1045	222.6	27.3	192.0	19.7	0.62
1015	218.7	32.3	182.8	24.0	0.62
1020	211.1	13.7	196.5	7.3	0.50

Table 2.2.9: Measurement results and total system efficiencies.

From table 2.2.9 it can again be observed that the efficiencies increase with both loading and rotational speed. Using these data, an attempt was made to analytically determine the maximum power ratio, α, that can be started. Recognizing that for constant excitation assuming identical DC-machines running at the same speed:

$$\alpha = \frac{I_{a,c}}{I_{a,t}} \tag{2.10}$$

$$= \frac{P_{mech,c}}{P_{mech,t}} \tag{2.11}$$

$$\tag{2.12}$$

and

$$\eta_{tot} = \frac{P_{el,c}}{P_{el,t}} \tag{2.13}$$

it is obvious that:

$$\alpha_{max} = \eta_{sg}\eta_{sm} \approx \eta sg^2 \tag{2.14}$$

Where η_{sg} and η_{sm} are the efficiencies of the synchronous generator and -motor respectively, as illustrated in figure 2.2.5. Using equations 2.13 and 2.11 we get the relation:

$$\begin{aligned} U_{a,t}I_{a,t}\eta_{tot} &= U_{a,c}I_{a,c} \\ \alpha &= \frac{U_{a,t}}{U_{a,c}}\eta_{tot} \\ \alpha &= \frac{e_a + I_{a,t}R_a}{e_a - I_{a,t}R_a\alpha}\eta_{tot} \end{aligned}$$

Solving for α:

$$-I_{a,t}R\alpha^2 + e_a\alpha - \eta\left(e_a + I_{a,t}R\right) = 0 \tag{2.15}$$

Inserting the maximum turbine current for 1040 rpm, 40 A, using η_{tot} for the highest power in table 2.2.9, 0.62, into equartion 2.15 we get:

$$\alpha_{max} = 0.83 \tag{2.16}$$

Taking equation 2.14 into account, it implies that:

$$\begin{aligned} \eta_{SG}^2 &= 0.83 \\ \eta_{SG} &= 0.91 \end{aligned}$$

Referring to table 2.2.8 this is a bit high, suggesting that η_{tot} should be slightly lower for $I_{a,t} = 40A$. As a control, the data from the 1045 rpm row if table 2.2.9 was inserted into equation 2.15. This gave $\alpha = 0.75$, whilst $\frac{19.7}{27.3} = 0.72$. The deviation is 4% and should be well within the margin of measurement error. An experimental exploration of the system's ability to start at different power loadings will be performed in section 2.3.

2.3 Shop model start-up

In this section the results from the laboratory start-up experiments will be presented and discussed in light of theory and sources of errors. The effects of increasing inductance between the generator and motor, as well as the ratio of compressor power to turbine power has been investigated.

2.3.1 Low frequency start-up

Low frequency start-ups as described in sub-section 1.1.3 were performed for a multitude of different conditions. The most important results are presented in the following.

No inductance

Initially, start-up of the machines was attempted without any inductance between the machines. The machines were coupled together with the contactor closed and their rotors magnetized. It became apparent that the motor would not start if its field current was too large. This would result in motor rotor slamming back and forth and the generator not being able gain speed. Eventually start-up was achieved with a generator excitation current approximately twice that of the motor. In absence of a proper voltage controller, a step increase in motor excitation was made as the system accelerated past 300 rpm. This was necessary in order not to loose synchronism as load torque increased at higher speeds. Figure 2.3.1 shows the generator and motor speeds during low frequency start-up without any line inductance and with $\alpha = 0.5$.

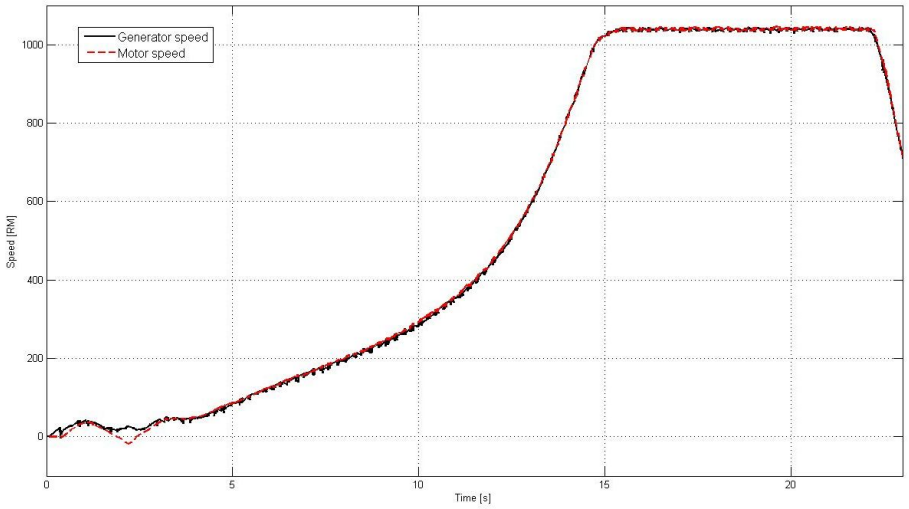

Figure 2.3.1: Generator and motor speeds. No inductance. $\alpha = 0.5$

In figure 2.3.1 it can be observed that synchronization is achieved after one pole slip, and that the system reaches rated speed after approximately 15 seconds. Figure 2.3.2

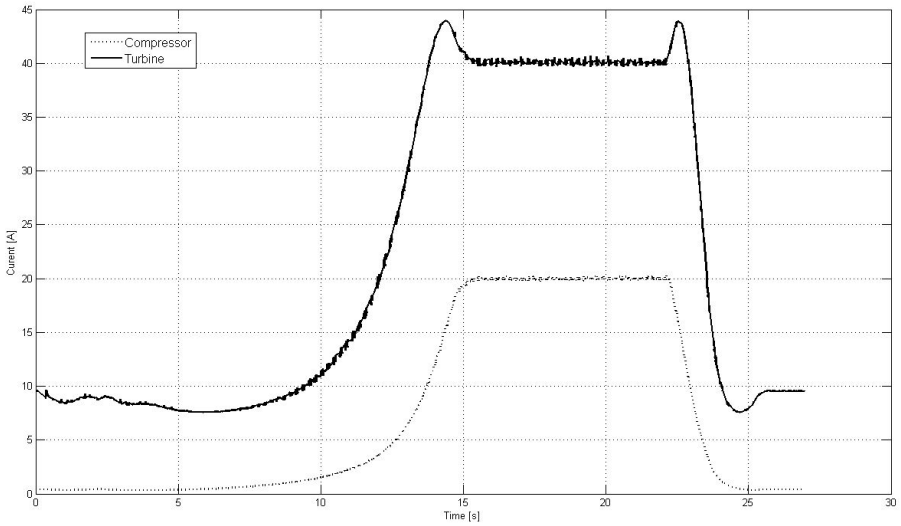

Figure 2.3.2: Output from maximum current. No inductance. $\alpha = 0.5$

shows the output from the maximum current loop illustrated in figure 2.1.5. Observe that for α=0.5, the output current limit for the compressor machine is half that of the turbine machine at rated speed.

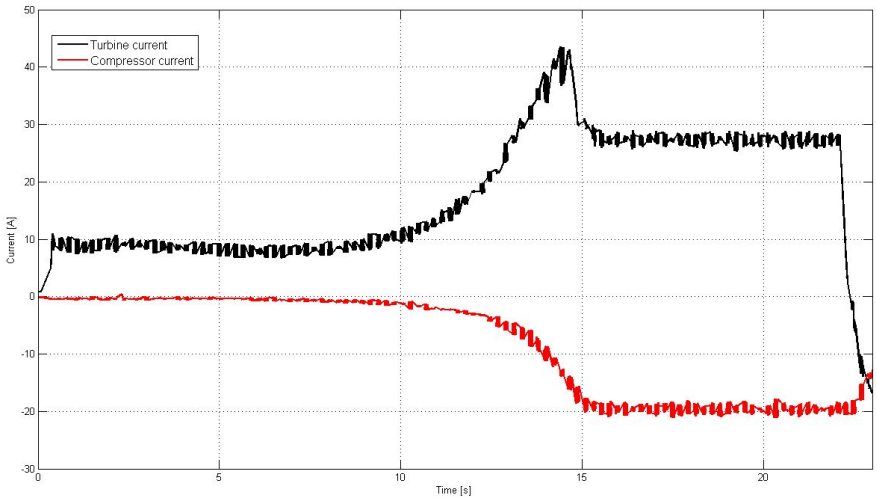

Figure 2.3.3: Turbine and Compressor current. No inductance. $\alpha = 0.5$

Figure 2.3.3 shows the actual DC-machine armature currents as measured. When comparing figure 2.3.2 and figure 2.3.3, it can be seen that the turbine machine is feeding the 20 amperes drawn by the compressor machine, in addition to losses. In this context it should be remembered that the DC-machines are running at the same speed, and that current thus is analogous to power.

Without any inductance between the machines the highest machine ratio, α, for which start-up was successful, was 0.75. Figure 2.3.4 shows the speed run-up for α=0.75

(left) and 0.8 (right). Note that for $\alpha = 0.8$ the system does reach a stable state and the system does not loose synchronism. The attempt is regarded as failed becaused the system does not reach its target speed of 1040 rpm. This is due to the drooping shape of the torque-speed characteristic for the last 100-150 rpm of the speed range. The SIMOREG speed controller is simply not capable of reaching its reference speed with the maximum current available to the DC-machine from the turbine characteristic, causing it to find a new steady state at a somewhat lower speed. The effect is readily visible in figure 2.3.5. Even though starting with $\alpha = 0.8$ was unsuccesful, later experiments will be conducted with 0.8 as the maximum. This is done to ensure that the system performance is squeezed to the limits of stability.

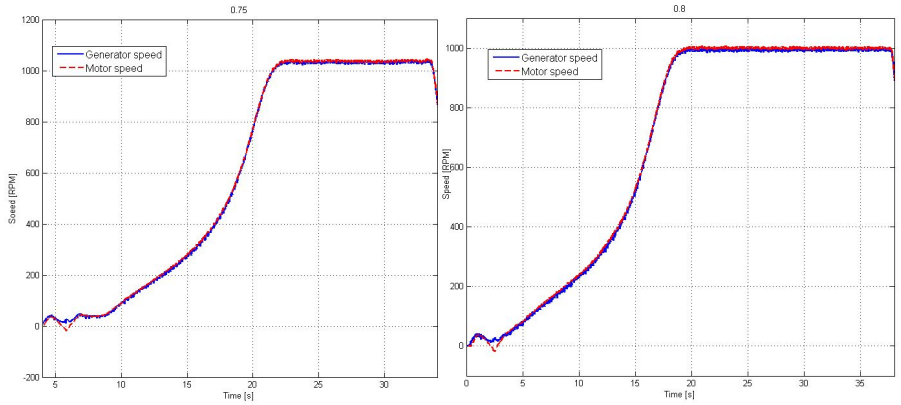

Figure 2.3.4: Generator and motor speeds for α=0.75(left) and 0.8(right)

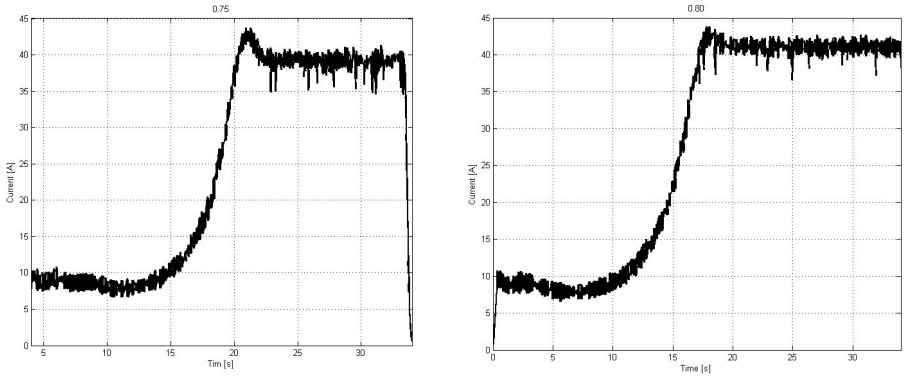

Figure 2.3.5: Turbine current for α=0.75 and 0.8

Line inductance

Not surprisingly, with the inductance between the machines increasing, it was eventually necessary to increase excitation currents. The step increase in motor excitation current was increased and a step was applied to the generator excitation as well. Figure 2.3.6 shows the generator- and motor voltages for an attempt on an α=0.8 start with two inductor levels engaged. To the left one can see the system collapse as generator excitation is too low, and to the right a successful start-up with modified excitation is shown. Figure 2.3.7 shows the speeds for the same run-ups. It should be noted that the time scales on the voltage- and speed measurements are not synchronized. This is due to the voltage being recorded with a separate data logger that needed to be started manually as the simulation is started, thus the zero-points are shifted.

Note that in figure 2.3.7 the speeds before collapse and steady state speed reached after the adjustments is more or less the same as in the run-up shown to the right in figure 2.3.4, implying that the active power balance is more or less unchanged by the inductor.

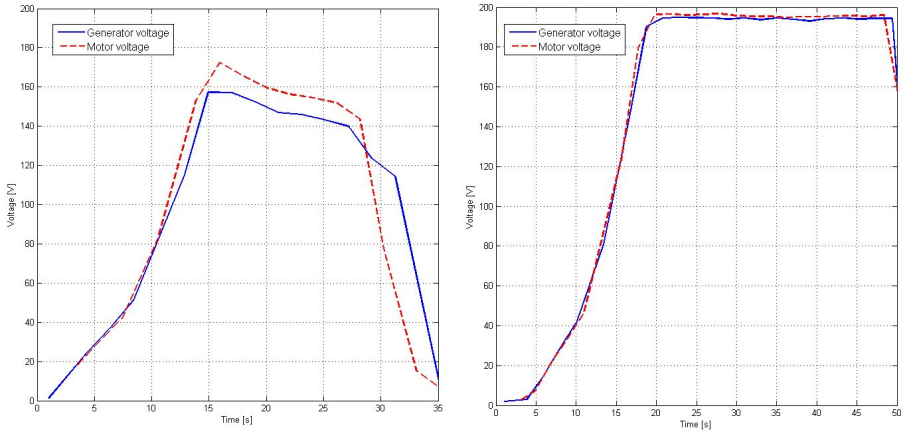

Figure 2.3.6: Machine voltages for α=0.8 and 2 inductor levels.

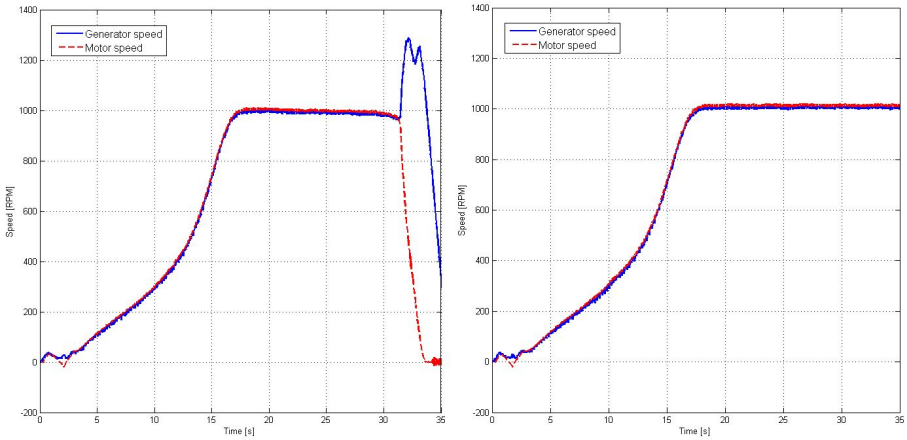

Figure 2.3.7: Generator and motor speeds for α=0.8 and 2 inductor levels.

Start-up was successfully achieved at four inductor levels for α=0.55. Figures 2.3.9 and 2.3.8 shows the voltages and speeds for the individual run ups using α=0.55 (left) and α=0.55 (right). However, it is in the opinion of the author that α=0.55 at four inductor

levels in no way should be regarded as the technical limit for low frequency start-up, as it was done using crude methods of excitation control. More thorough investigations using professional voltage control equipment should be able to push the inductance and active power starting capability further. It appears start-up with line inductance is simply is a matter of supplying enough reactive power, and through more sophisticated voltage control the reactive power loading may be shared more efficiently between the machines. It has however been established that it is possible to start a 4.4 kW compressor with the torque-speed characteristic in question through a 43.2 mH satiable iron-core inductor.

As previously mentioned the inductor has a very low resistance and thus does not affect the active power situation. This can readily be seen in figure 2.3.8, where the system reaches reference speed at both α=0.55 and 0.6. In the event of a long sub sea three-phase cable, the line inductance may even be negligible due to the cable capacitance. In such a case it may be more interesting to look at the effects of resistance, which would be dominating at low frequencies, and reactive power surplus at higher frequencies. Unfortunately there was no time to perform experiments with resistance between the machines. However, an inquiry into the effects of resistance using simulation tools has been made in sub-section 3.1.4.

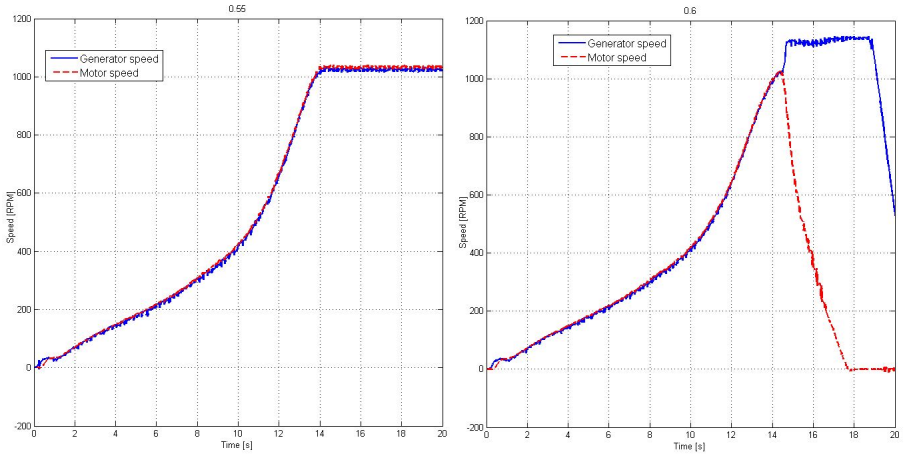

Figure 2.3.8: Generator and motor speeds for α=0.55 and 0.6 at 4 inductor levels.

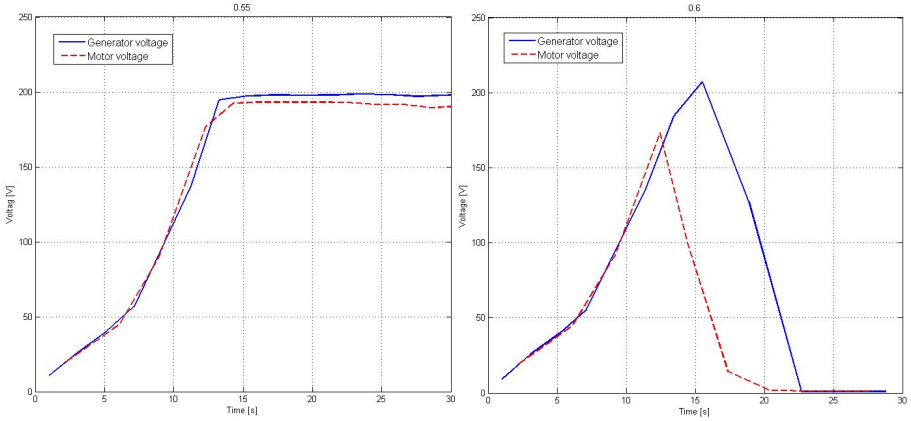

Figure 2.3.9: Machine voltages for α=0.55 and 0.6 at 4 inductor levels.

2.3.2 Partial frequency starting

When attempting partial frequency start-up, the generator was run at approximately 60% of nominal speed, i.e.≈600 rpm. The generator was magnetized so as to produce an open circuit voltage at ≈100V. An oscilloscope was trigged to capture the transient responses of the phase and field currents.

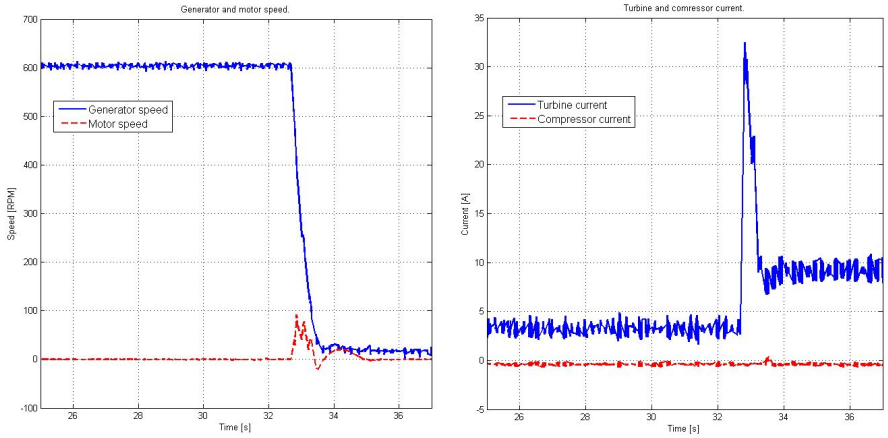

Figure 2.3.10: Machine speeds and compressor- and turbine currents. α=0.5

Figure 2.3.10 shows the generator and motor speeds together with compressor and turbine currents as a partial frequency start is attempted loaded at α=0.5. It is evident that the attempt is unsuccessful. As the contactor is closed the turbine is idling at 3-4 amperes, only supplying electric and rotational losses. It can be seen that as the motor initially picks up speed, the generator speed plummets. It appears the turbine-generator set is simply delivering its stored rotational energy to the motor-compressor set without ever transferring any power from the turbine machine to the motor. Figure 2.3.11 shows the motor stator- and field winding currents in the motor.

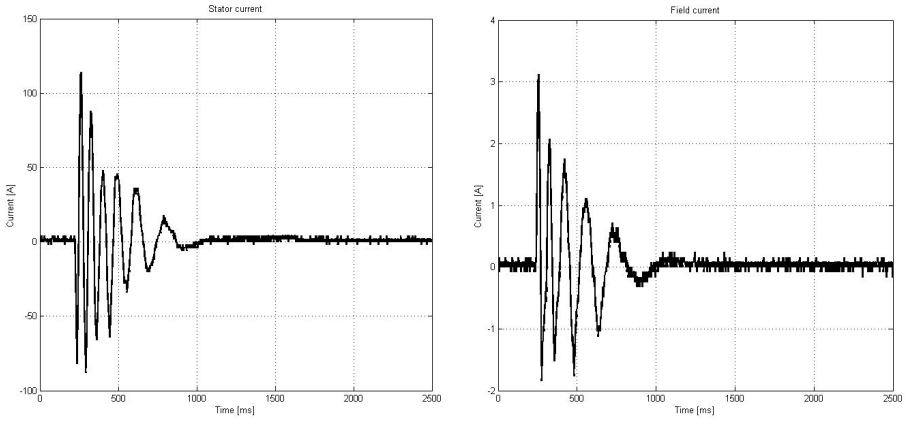

Figure 2.3.11: Stator (left) and field (right) currents in motor. α=0.5

As described earlier in sub-section 2.2.3, the machines are very similar and their inertias are assumed to be the same. This means that during the initial few milliseconds after engagement, any speed gained by the motor-compressor set is lost in the turbine-generator

set. Active power is not delivered to the system until the DC-motor drive control system recognizes that the turbine speed has dropped and increases the current. However, by the time the turbine current has responded, the speed has dropped significantly and the torque-speed characteristic now limits the current to a mere 10 A.

Consequently the Labview control system was modified so as to keep the turbine maximum current at the 600 rpm level. In this manner it would become clear if the turbine could halt the collapse if it did not loose torque as it lost speed. In figures 2.3.12 and 2.3.13 the modified scheme is shown to start the system. However, as the turbine-generator set still looses all but 100 rpm of its speed during the initial asynchronous acceleration, the start-up should not be regarded as successful.

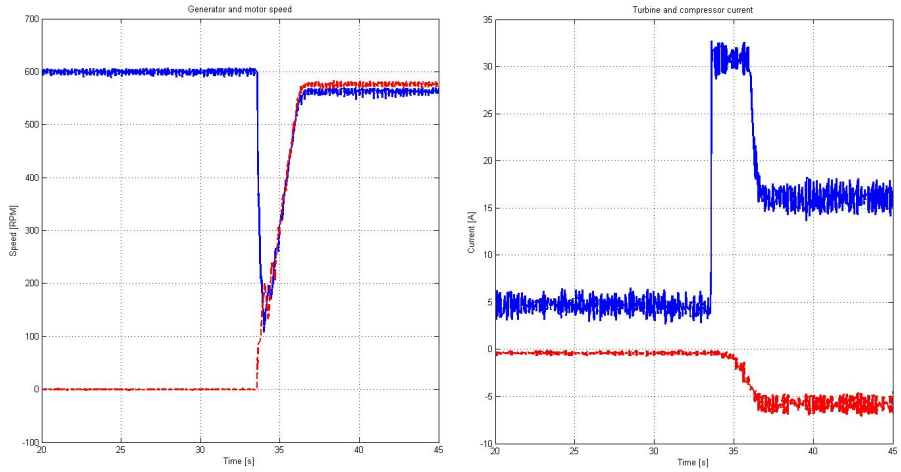

Figure 2.3.12: Machine speeds and compressor- and turbine currents. α=0.5

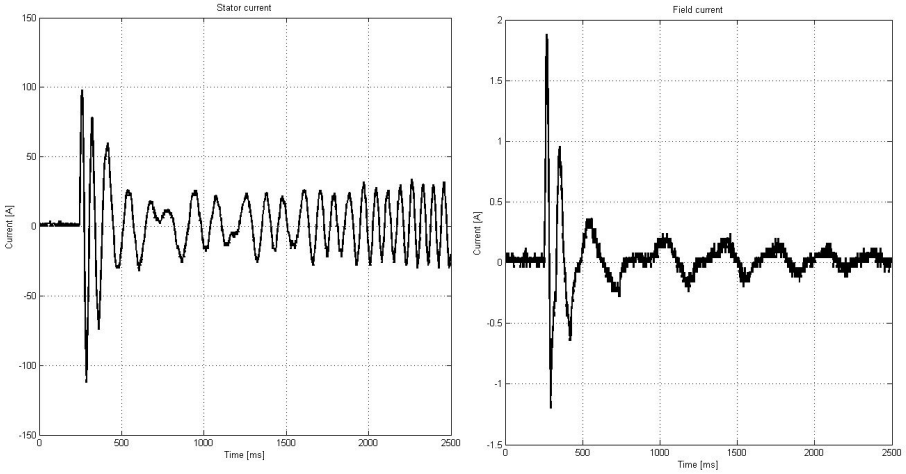

Figure 2.3.13: Stator (left) and field (right) currents in motor.

The failure of the partial frequency starting scheme is thus due to the small inertia of the generator and turbine, as well as the fact that control system needs speed error in order to react. Partial frequency starting thus appears unsuitable for any practical application without considerable difference in generator- and motor inertia. In addition, a control system should be in place to power up the turbine prior to engagement. Even in such a case it partial frequency starting would entail excessive strains on mechanical parts and is not recommended.

2.3.3 Back-to-Back soft start-up

During the soft start-up experiments, the generator was run idly at approximately 620 rpm while non-magnetized. The motor was at standstill with its field winding open circuited. The generator field current was then ramped manually up until an incremental increase in field current did not improve motor speed. At this point the motor field winding would engaged and synchronization attempted.

No inductance

The motor was successfully started in this manner at α=0.8 without inductance. After a successful start at α=0.8 further increases was regarded as unnecessary, as the experiences from section 2.3.1 tell us that after synchronization the machines will not reach target speed. Figure 2.3.14 shows the generator- and motor speeds, field current, motor voltage, and line current for a run up at $\alpha = 0.8$. Note that the field current is amplified 100 times in order to correspond with the axes and that the time scales are not interchangeable.

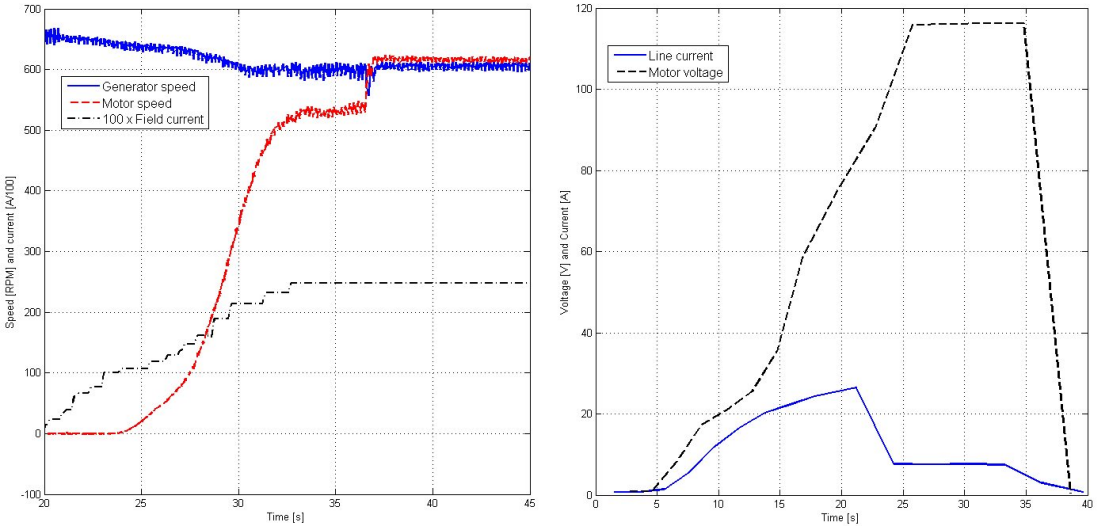

Figure 2.3.14: Machine speeds, amplified field current, motor voltage, and line current for α=0.8 and no inductance.

Line inductance

As line inductance increased, the voltage that the generator was able to maintain at the motor terminals decreased. Hence, the slip at which synchronization was attempted increased. This may be observed in figure 2.3.15, which shows the α=0.8 run-ups for 1 and 2 inductor levels respectively.

At three inductor levels it was no longer possible to successfully synchronize with higher α than 0.3 with successful synchronization. Please do observe in figure 2.3.16 that

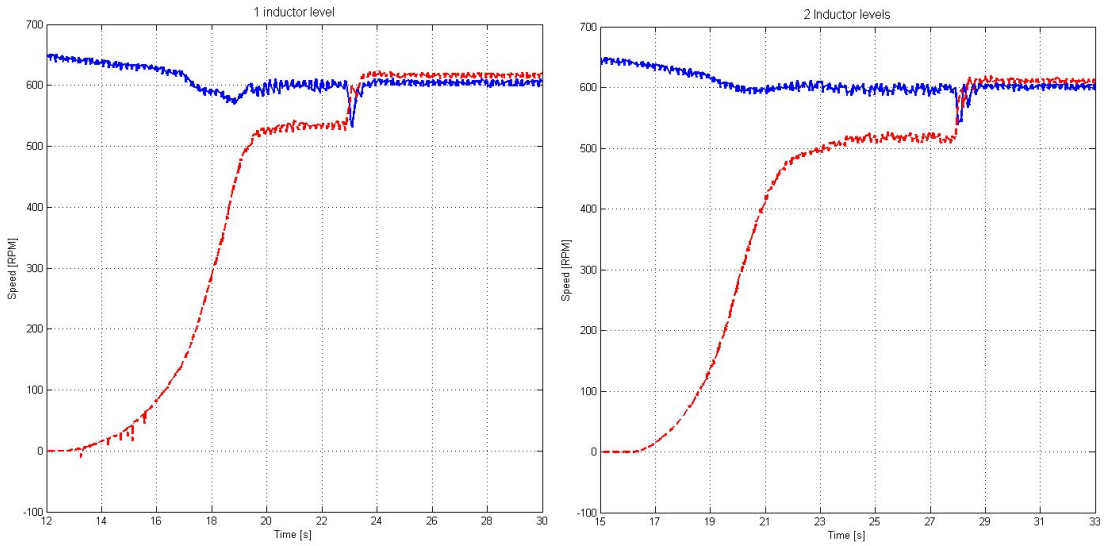

Figure 2.3.15: Generator- and motor speeds for α=0.8 at 1 and 2 inductor levels.

the slip at which synchronization is attempted has increased to ≈70-80 rpm, which is comparable to the right part of figure 2.3.15, even though the load considerably less. It may also be observed that the motor terminal voltage jumps from ≈50V to ≈125V as synchronization is achieved.

In order to verify that motor terminal voltage was the constraint, two small capacitor batteries were connected on the motor side of the inductor. Figure 2.3.17 shows the capacitor aided start for α=0.4. Note that the terminal voltage at synchronization has been improved, however only just, even though active power demand is now greater. Capacitor aided starting was not achieved for α=0.5.

It appears that soft starting is more sensitive to line inductance than low frequency starting. This is quite intuitive, as the entire reactive load now has to be supplied by the generator. The situation is partially redeemed by reducing frequency and hence reducing both the amount of active power that needs to be transported and the effective line reactance.

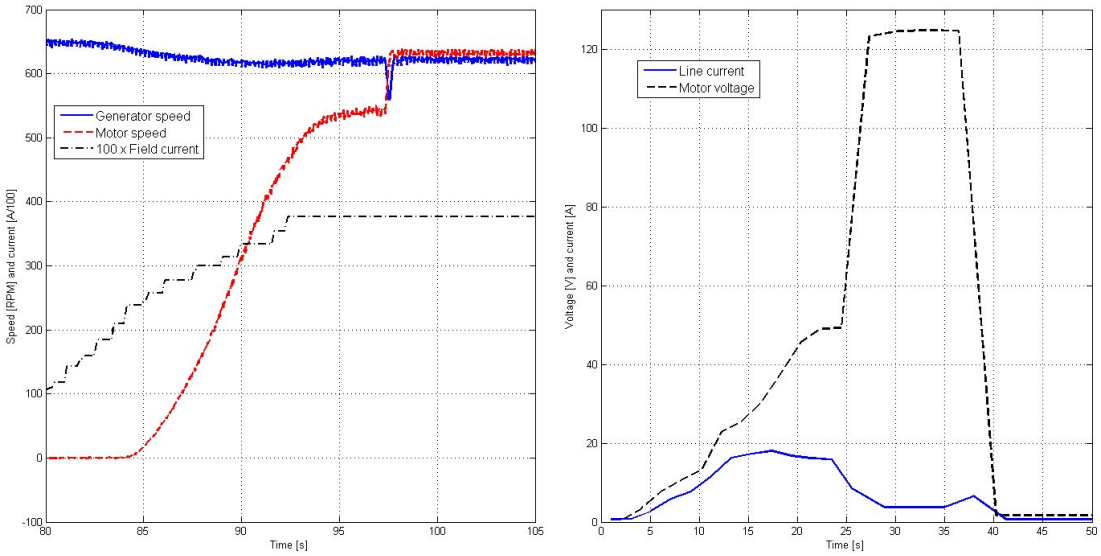

Figure 2.3.16: Machine speeds, amplified field current, motor voltage, and line current for α=0.3 and 3 inductor levels.

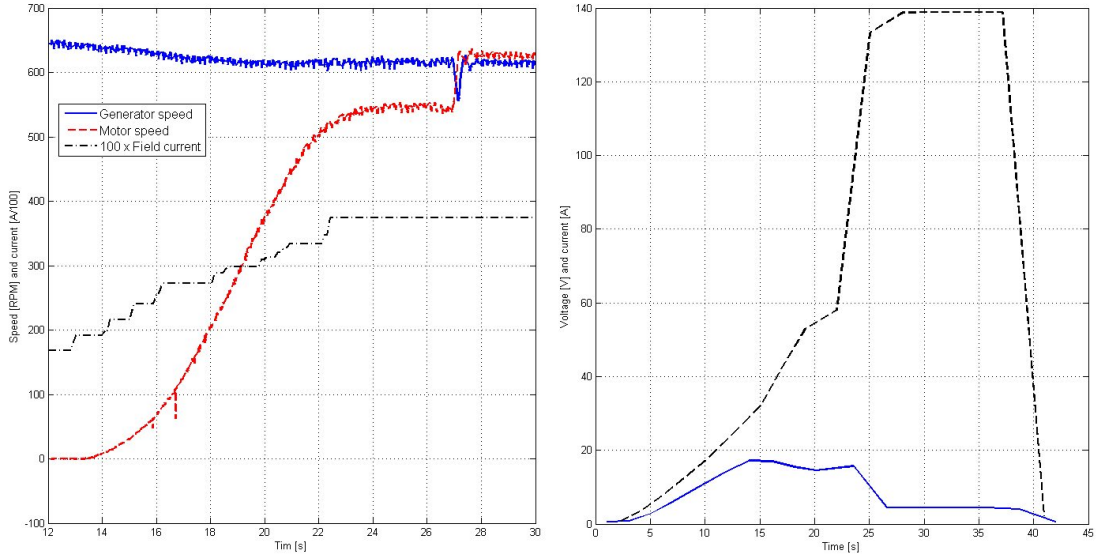

Figure 2.3.17: Machine speeds, amplified field current, motor voltage, and line current for α=0.4 and 3 inductor levels with capacitor in parallel.

2.3.4 Shop model conclusions

Low frequency starting with zero inductance between the generator and motor, was achieved with a compressor to turbine power ratio, α, of 0.75. For higher values of α the system halts at a slightly lower speed where there is more turbine torque available. A compressor loading of $\alpha = 0.75$ corresponds to 6 kW at 1040 rpm. The generator excitation should be almost twice that of the motor. If the motor excitation is too high, the poles will slip continuously and the rotor can be seen to rock back and forth.

Line inductance was shown to only have a slight detrimental effect on start-up. Quite clearly excitation levels needed to be adjusted in order to properly satisfy increasing reactive power demand. Yet, once a simple excitation controller was in place, starting of an α=0.8, or 6.4 kW-, model compressor to a slightly reduced speed was achieved with two inductor levels engaged. This corresponded to 13.2 mH at unsaturated- and 10.97 mH at saturated conditions, or 2.82/2.34 Ω @ 34 Hz.

The highest α and inductance that was successfully started was 0.55 at 4 inductor levels, corresponding to 4.4 kW and 43.2/37.26 mH, or 9.23/7.96 Ω @ 34 Hz depending on saturation. However, it is in opinion of the author that through more sophisticated excitation control, higher values of α could have been started.

Partial frequency starting was not achieved for any values of α, including zero. It is concluded that partial frequency starting should not be attempted in the described manner unless the inertia of the motor is significantly less than that of the generator. In addition a control system should be in place to give the power up command to the turbine in advance of the engagement. Start-up would then by done as the generator is accelerating. However, it does appear unlikely that this method can be competitive with any of other two in question.

Soft starting to 620 rpm was achieved successfully for α=0.8 with 0, 1, and 2 inductor levels engaged. As the voltage drop across the inductors increased, the maximum motor terminal voltage that the generator was able to produce decreased. Hence, the slip speed at which synchronization was attempted increased with inductance.

At three inductor levels the highest α that could be started was 0.3. At any higher value, synchronization was unsuccessful. The reason was that the generator could no longer supply the amount of reactive power needed to achieve sufficient motor voltage for starting. This was verified by successfully starting α=0.4 with a capacitor bank connected in parallel at the motor side.

Chapter 3

Starting simulations.

In the following, the work that was performed using Matlab-Simulink will be presented. The chapter contains a verifaction part, in which the efforts put into parameter estimation will come to its right, and a full scale part, in which more realistic parameters will be used.

3.1 Verification

During the master thesis pre-project conducted autumn 2008, a simulation model was established to investigate the possibilities of on-load low-frequency starting of an LNG-compressor drive. This model will be revisited in this section, where its validity will be tested as it is compared to the laboratory scheme. Due to time constraints, efforts were concentrated on verifications of low-frequency start-up simulations.

The simulation model consists of two PU-fundamental synchronous machines from the Simulink Block library. Their stators were connected together, with a discharge resistor in parallel due to problems regarding simulations of stiff systems [15].

The turbine was modelled as PI-controller which fed pu torque to the synchronous machine. The torque signal ranged from 0-1 with delivering 0.8 at rated speed, and was passed through a dynamic saturation block in orde to ensure that it did not exceed the values determined by the torque-speed characteristic. A rate limiter was included between the PI-controller and the dynamic saturation block in order to simulate the gas turbine response time. The compressor was a simple second order polynomial block, recreating the torque speed characteristis of the sub-cooling compressor.

The generator had a voltage controller and a power system stabilizer, while the motor excitation was controlled by a PI-controller towards unity power factor.

For more detailed information on the simulation model, general reference is made to the pre-project automn 2008 [9].

	Generator	Motor
X_d	1.228	0.44
X_q	0.315	0.283
$X_d^{'}$	0.261	0.124
$X_q^{'}$	0.315	0.283
$X_d^{''}$	0.242	0.11
$X_q^{''}$	0.346	0.259

Table 3.1.1: Per unit synchronous machine parameters

3.1.1 Shop model data: Verification

The machine parameters were converted to per unit for the Matlab-Simulink input. A per unit system was established choosing:

$$U_{base} = 230 \text{ V} \quad S_{base} = 18 \text{ kVA}$$

Giving:

$$I_{base} = \frac{18kVA}{\sqrt{3} \cdot 230V} = 45.2A \quad Z_{base} = \frac{230V}{45.2} = 5.08\Omega$$

Enabling pu values of the parameters from section 2.2 to be input to the machine models as shown in table 3.1.1. In order to implement the laboratory setup in the simulation model, some changes had to be made. As mentioned earlier, the DC-motor drive in the laboratory had a proportional speed controller. Hence the turbine model had to be changed correspondingly, removing the integral effect and the rate limiter. After all, the drive can be seen to act fast in figure 2.3.12 once an error signal is detected. Moreover, upon introducing a line inductance between the machines, another parallel resistor had to be provided. This is because the synchronous machines in the Simulink block library are modelled as a current source and thus may not be placed in series with an inductor [15].

The synchronous machine model used in the simulations does not make use of $I_{f,rated}$. Instead it refers rotor quantities to the stator and they are converted to pu using machine power- and voltage rating. Thus 1 pu V_f produces 1 pu I_f which again produces 1 pu V_t at zero load conditions. In order to emulate the machines in the laboratory, the logged field currents were divided by their respective rated field currents. These are the values found in sub-section 2.2.5, and the results fed to the V_f input of the synchronous machine [15]. In this manner V_f is synthesized from the laboratory I_f:

$$V_{f,g} = \frac{I_{f,g}}{1.56}$$
$$V_{f,m} = \frac{I_{f,m}}{1.08}$$

3.1.2 Simulation results - Collapse

A reconstruction of the collapse at α=0.8 with two inductor levels, described in section 2.3.1, was made in the simulation model. It soon became apparent that the system was quite sensitive to saturation of the line inductors. If the inductance was set at any of the three values available for two inductor levels in table 2.2.6, the system would collapse before or immediately after reaching target speed. In order to replicate saturation conditions in the line inductance a curve fit was made from the three data points for two inductor levels in table 2.2.6. Unfortunately, due to a lack of ports and prioritization of motor and generator voltage, the current was not logged in the original run. Thus, in order to determine the appropriate value of the line inductance, it was set low so that starting was stable at the target speed. Then the inductance was gradually increased until a collapse occured. This happened at L=9.05 mH, which corresponded to a current of approximately 27.65 A.

Figures 3.1.1 and 3.1.2 shows the simulated and measured motor- and generator voltages and -speeds as the system collapses during an attempt on α=0.8 and with two inductor levels engaged. Note that upon collapse the laboratory run is stopped manually due to safety concerns while the simulation continues steadily. Except for this the results are fairly similar.

It can be seen that everything in the simulations happens faster than in the lab. That is, the system reaches the critical speed faster and the collapse happens earlier. It can also be seen that the voltages are somewhat higher in the laboratory run, suggesting that the approximations made to replicate the field currents are a little shaky. Also the approach to simulate saturation of the inductor, has some inherent weaknesses, as it is not flexible to the mutual effects between current, inductance and reactance. It is assumed that a proper satiable mutual inductor model in Simulink would produce different results. That being said, it is in the opinion of the author that the tendencies and shapes of the plotted curves are so similar that it is reasonable to conclude that the breakdown is caused by the same phenomenon. This hypothesis is strengthened by the fact that the failure occurs at approximately the same speed and presumably at the same excitation levels.

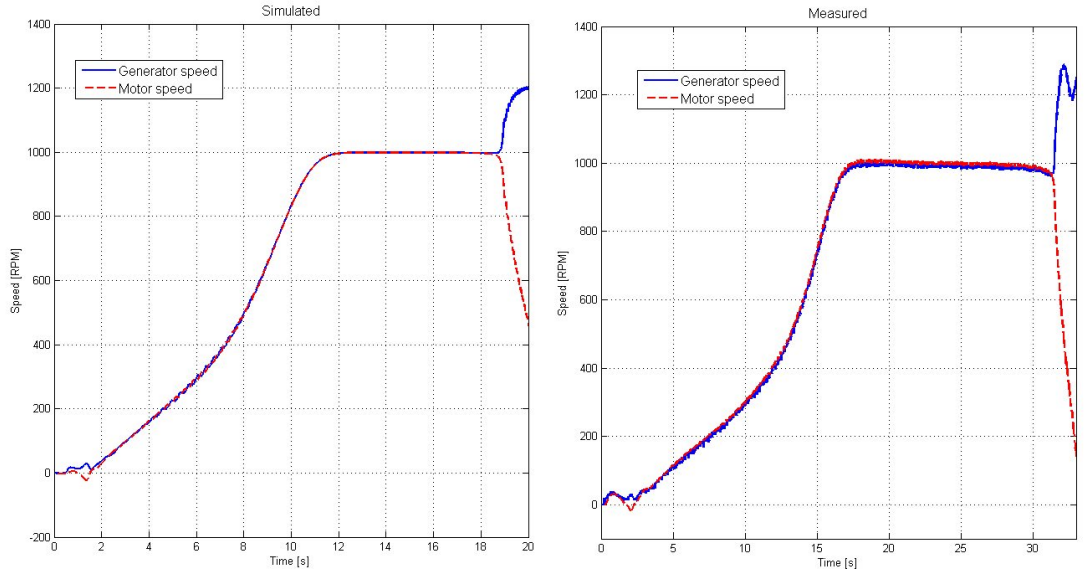

Figure 3.1.1: Simulated(left) and measured(right) speeds for a failed run on α=0.8 and with two inductor levels.

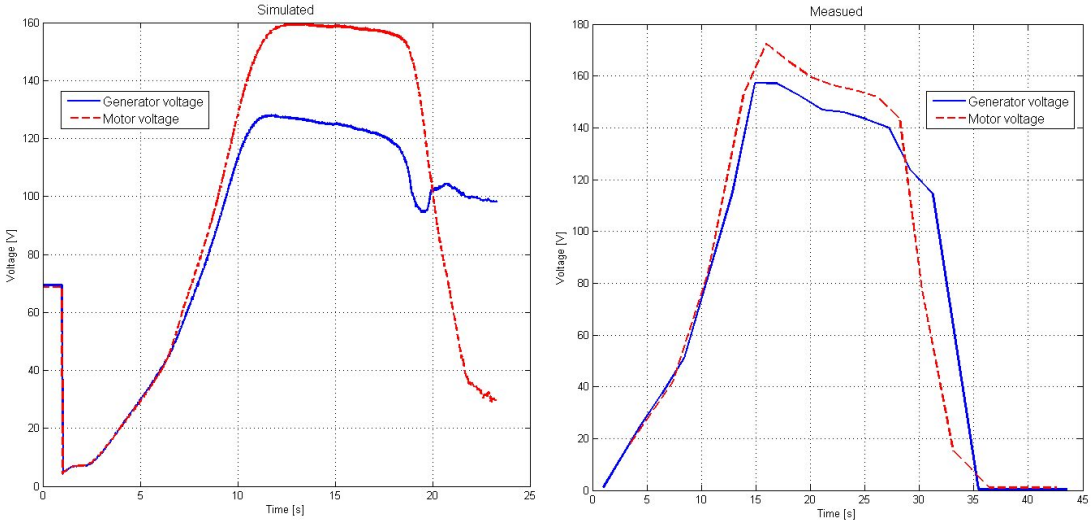

Figure 3.1.2: Simulated(left) and measured(right) voltages for a failed run on α=0.8 and with two inductor levels.

Collapse phenomenon

Taking a look at the situation immediately after the system reaches a stationary speed, which is approximately where the voltages peak, a phasor diagram of the system as seen from the motor can be drawn. For t=12.8 seconds the following data was obtained graphically:

$$\begin{aligned} |I| &= 28A \\ |V_m| &= 159.5V \\ P_m &= 0.265pu = 6030W \end{aligned}$$

It thus follows from

$$P_m = \sqrt{3}V_m I\cos(\phi)$$

that ϕ ≈39. The power factor can be seen to be leading, as the motor is delivering reactive power. Figure 3.1.3 shows a schematic of the phasor diagram and figure 3.1.4 shows the motor terminal voltage and -output reactive power as well as the phase current for the 10 seconds leading up to the collapse.

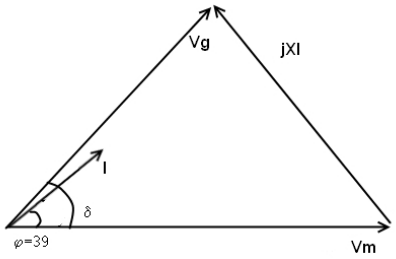

Figure 3.1.3: Approximate phasor diagram for the collapsing system as seen from motor.

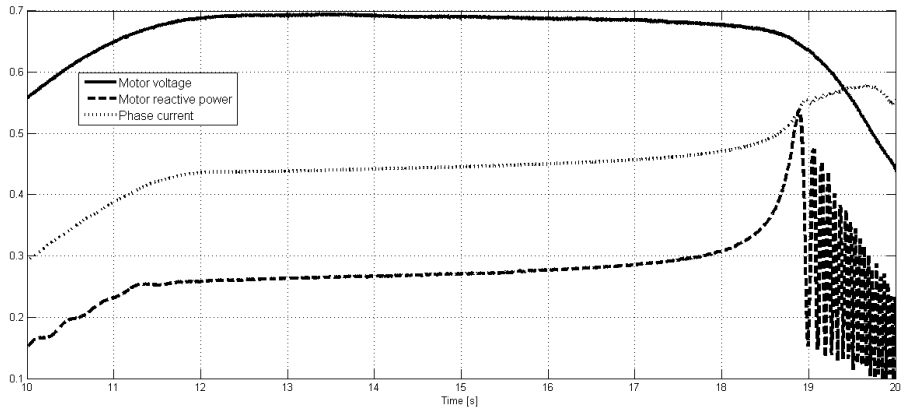

Figure 3.1.4: Phase current and motor terminal voltage and -output reactive power.

From figure 3.1.4 it may be observed that as the voltage starts its descent, the current increases with a similar shape. This is necessary in order to maintain the active power at a constant level, as the motor speed and hence the compressor power is relatively constant. We can also see the reactive power output increase steadily throughout the

course of the breakdown, and then more violently towards the end. This is due to the reactive power demand increasing proportional to the square of the current increase.

An explanation of the collapse could be that as the system finishes acceleration and settles at approximately 1000 rpm, the currents in the motor field- and damper windings die out. The synchronous torque is slightly too small and the load angle, δ, starts to increase. It can be seen from figure 3.1.3 that as δ increases, so must the current. Thus, when the current increases the reactive power demand increases and voltage decreases. When the voltage decreases this leads to a loss of electromagnetic torque, as described in equation 1.18. This further increases the power angle to make up for lost torque, which in turn increases the current and so forth. The system has now entered a voltage driven collapse.

As we can remember from sub-section 1.2.4, the system is considered unstable when an incremental decrease in voltage leads to a deficit of reactive power. This corresponds with the events earlier described as constituting a voltage collapse.

3.1.3 Simulation results - Restoration

By remedying the situation in the same manner as it was done in the laboratory and described in section 2.3.1, i.e. increasing the generator excitation, more light may be shed on the viability of the simulation model. Figures 3.1.5 and 3.1.6 shows the results of the simulations with modified excitation and their corresponding measured lab results.

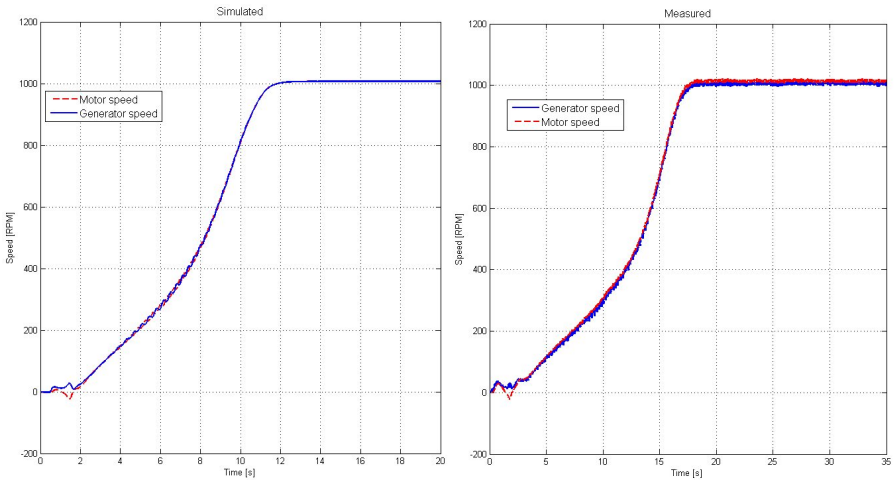

Figure 3.1.5: Simulated and measured speeds for a successful run on α=0.8 and 2 inductor levels, after modifying excitation.

Upon inspection it is immediately obvious that the simulated voltages to the left in figure 3.1.6 are lower than that of the laboratory run on the right. Furthermore, it can be seen that the generator voltage is higher than the motor voltage and not vice versa, as is the case in the laboratory run. This goes a long way to support the suspicion that the assumptions made on excitation are in need of improvement. It would seem that the models in Matlab Simulink does not allow the field resistances and -inductances to

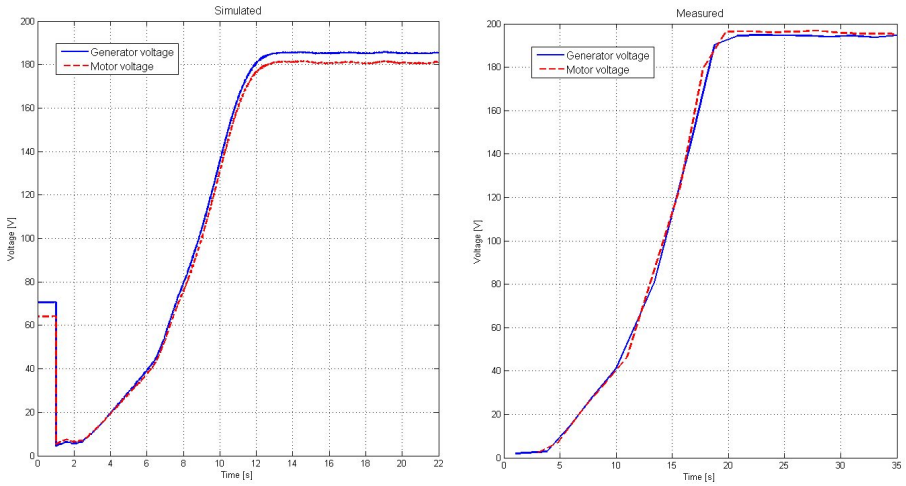

Figure 3.1.6: Simulated and measured voltages for a successful run on α=0.8 and 2 inductor levels, after modifying excitation.

be different for the two machines, which they most likely are.

When, in an attempt to verify this hypothesis, the motor excitation was increased, the voltage on the motor side did not surpass that of the generator until its field voltage did. The most likely source of error is thus probably in the synthetization of field voltages from measured field currents as described in sub-section 3.1.1.

Inertia

In an attempt to offset the difference in acceleration time, a power balance approach was adopted. The speed reference was set to 1 pu and the proportional gain in the controller simulating the SIMOREG or turbine was increased, ensuring that it would not hold back. This way, when the machines stop accelerating it is necessarily because the drooping torque-speed characteristics in the turbine max-torque block delivers the same amount of active power as the compressor and losses consume. The synchronous machine friction factor was then increased until the system only barely reached 1000 rpm as the laboratory run-up shown to the right in figure 3.1.5 and the turbine torque function showed the same simulated current as the lab measured output from the maximum current. This ensures that the active power balance is identical.

Figure 3.1.7 shows the measured and simulated turbine machine current for a friction factor of 0.095 pu. In this case the active power and speed is approximately the same in the laboratory and in the model. If this is the case, acceleration time should be a matter of inertia alone. Machine inertia was then increased until the simulated acceleration time matched that of the laboratory. Figure 3.1.8 shows the simulated and measured speed for the α=0.8 and 2 inductor scenario, with friction and inertia modified.

The inertia constant, H, is now 0.575. The deviation from the estimated 0.506 is 13.6%, which corresponds to an inertia, J, of 0.841. Revisiting figure 2.2.3 describing the inertia

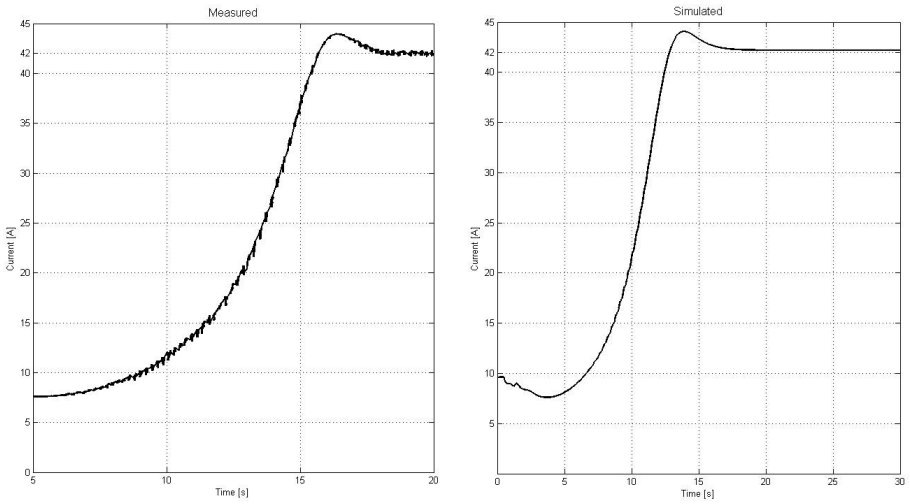

Figure 3.1.7: Measured and simulated turbine machine current after adjustment.

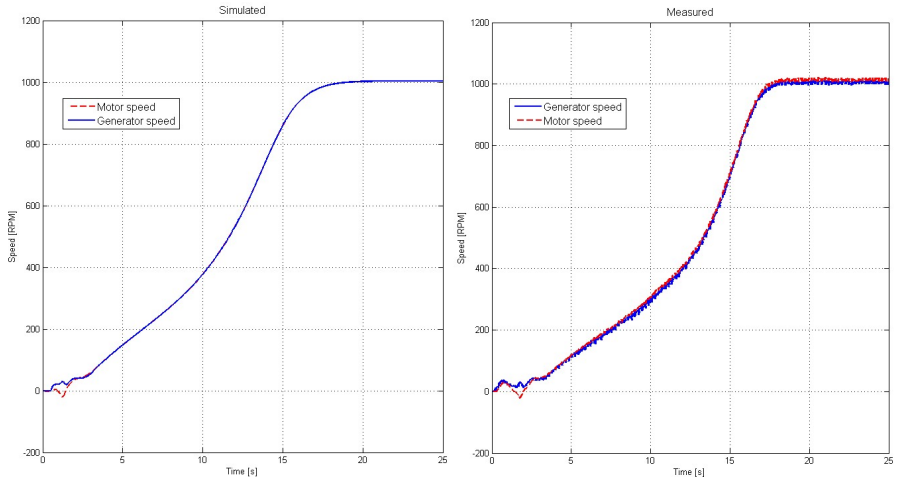

Figure 3.1.8: Measured and simulated turbine machine current after adjustment.

estimation process and assuming that the linear speed change is correct, this translates into an accelerating dc-motor current of 24.98 A. Upon inspection of the figure this does not seem very likely. However, the inertia estimation was done on an unexcited machine and hence does not take stator iron eddy currents into account. These losses could be considerable as the actual run-ups are done using rather high excitation values, i.e. $\geq$ 1 pu. It has been decided that there is little expediency in delving further into these matters.

The results presented in the above and illustrated in figure 3.1.8 show that comparable results can be achieved when the active power balance an inertia is correct. In order to obtain identical acceleration patterns, the losses need to be correctly distributed among friction, which is proportional to speed, windage, which is proportional to the square of the speed, and stator iron losses, which is proportional to speed at a certain excitation level.

3.1.4 Effects of resistance

It was initally assumed that the effects of resistance in the laboratory would be negligible. However, it became apparent during the course of the investigations in the above, that this was not necessarily true. As mentioned earlier, there was no time to go back to the lab to experiment with line resistances. Hopefully the simulation inquiry presented in the following will shed light on the issue.

Figure 3.1.9 shows a failed start with a line resistance of 0.57 Ω. The generator excitation is 2.3- and motor excitation is 1.5 pu.

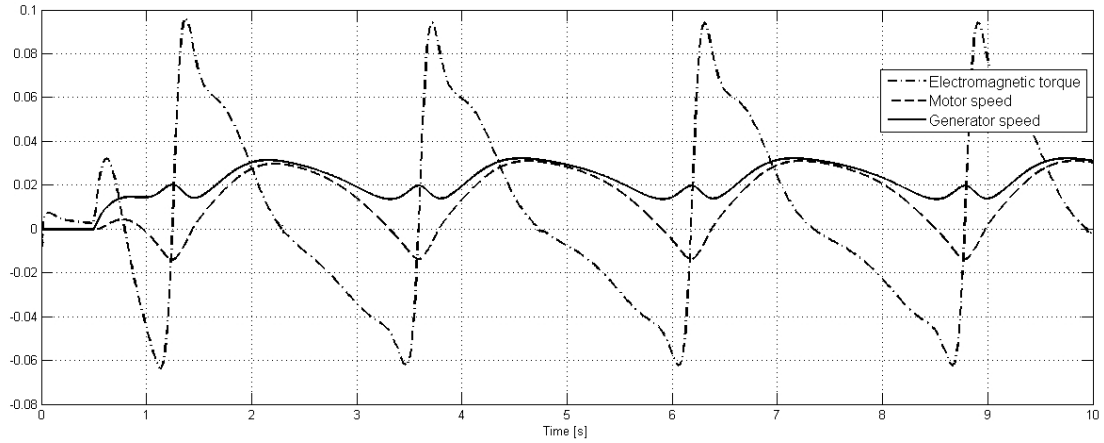

Figure 3.1.9: Motor speed, electromagnetic- and load torque, with insufficient excitation.

From figure 3.1.9 it can be seen that the start-up is inhibited by a series of pole slips. It is evident that T_{em} peaks as the sum of the synchronous and asynchronous torque reaches its highest point, accelerating the motor. As the system almost reaches synchronization, the torque drops to almost zero and then slips into negative territory. Repeating equation 1.18:

$$T_2 = \frac{1}{\omega_2}\left[\frac{E_1 E_2}{|Z|}\sin(\delta + \kappa_z) - \frac{E_2^2 R}{|Z|^2}\right]$$

where T_2 is the electromagnetic torque of the motor, it is clear that $\delta + \kappa_z$ has passed 90° during acceleration. It is thus necessary to increase the synchronous torque.

From the first term in equation 1.18 it can be seen that we have two options for increasing developed synchronous electromagnetic torque: Increasing E_1 or increasing E_2. However, increasing E_2 will also increase the magnitude of the negative second term, while E_1 only affects the positive. Figure 3.1.10 shows a failed start where generator excitation has been increased to 2.4 and motor excitation has been kept at 1.5.

The motor now manages to keep synchronism, but the system evidently fails to accelerate beyond a very low speed. This is due to the dip in available torque from the turbine in the low end of the torque-speed characteristic. When an increment was added to the maximum torque feed, effectively shifting it upwards 0.01 pu, the system reached a somewhat higher speed before settling. When it was shifted by 0.02 pu, this was enough

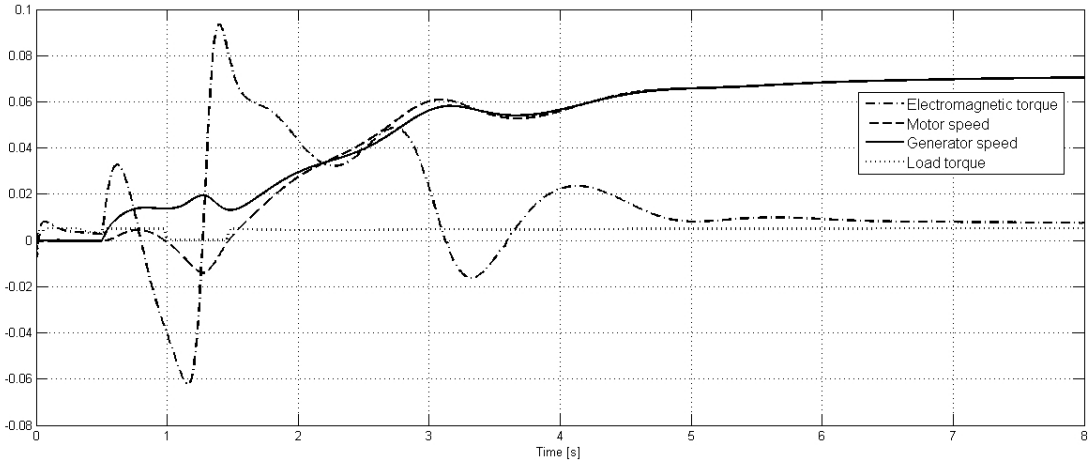

Figure 3.1.10: Motor speed, electromagnetic- and load torque, with modified generator excitation.

to bring the system past the dip, and successful starting was achieved. The reason for this is that the active power lost in the resistor together with losses in the machines and the load, corresponds with the available prime mover power at that speed. In short more power has been made available to the system to cope with losses and acceleration.

However, it seems intuitive that it is possible to decrease the amount of power lost in the resistor by increasing the voltage at the motor side and, hence, reducing the current. Figure 3.1.11 shows the successful attempt at starting of without shifting the torque available but by increasing the motor excitation to 1.6.

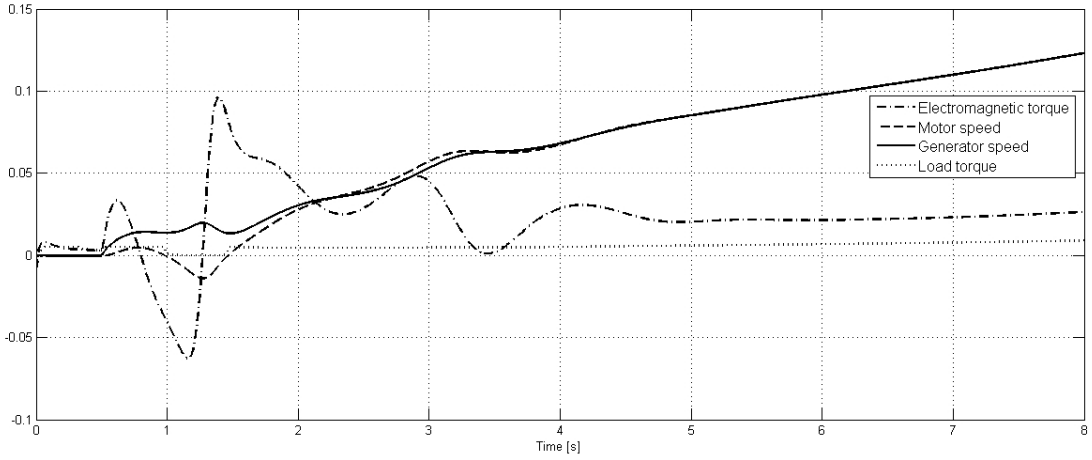

Figure 3.1.11: Motor speed, electromagnetic- and load torque, with modified generator- and motor excitation.

Quantitatively, the first term in equation 1.18 has increased more than the second term, resulting in a net increase in electromagnetic torque. Upon furher increases in motor excitation the acceleration time decreases as a consequence of increased electromagnetic torque, until problems with convergence is encountered at 1.72 pu motor excitation.

The largest line resistance for which low frequency start-up was successful was 0.58 Ω or 0.1142 in pu of the synchronous machine rating. In comparison the resistance of a typical $72kV3 \cdot 1 \cdot 630mm^2$ sub sea cable rated at 50 MW is 0.04 Ω/km. Using 66 kV and 50 MVA as base values, this corresponds to $2.65 \cdot 10^{-4}$pu. A resistance of 0.1142 pu then represents 430.8 km which is quite sufficient to conclude that resistance will not be the constraining factor. It should also be noted that the prime mover power rating is only 44% of that of the generator.

In light of the above, the resistance from terminal to terminal was measured by means of a ohmmeter. It was 0.245 mΩ, which is 43% of the maximum resistance successfully started, 0.57 Ω, and hence not negligible at all. Because it would have entailed a great deal of strain in order adept the field currents as in section 3.1.3, no further efforts were made to incorporate the actual resistance in the verification model.

The findings in the above indicate that larger scale experiments could be simpler than those performed in this thesis. This is because the per unit resistance decreases with increasing machine rating. For example the per unit resistance at 70°of the ABB Motorformer used in the full scale simulations is 0.0014. Also the fact the prime mover in the above was very small compared to the synchronous machines bodes well for future up-scaling.

3.1.5 Verification conclusions

The means by which excitation voltage in the simulation model was determined from laboratory field current may inaccurate. Without proper knowlegde of the machine transformation ratio, any actual comparison between simulated and actual rotor field current is not possible. The accurate simulation of such quantities requires more sophisticated models than those available in the Simulink library [16]. Even with these limitations, the model seems to give proper results on other accounts.

The model has been shown to behave in very similarly to the laboratory set up during voltage collapse for the same conditions as in the laboratory. The means of mending the collapse in the laboratory also mended the collapse in the simulation model.

Discrepancies were found in acceleration- and collapsing time, however satisfactory results were obtained by replicating losses using a power balance approach and increasing inertia. Line resistance was found to adversely affect synchronous start-up by causing a voltage drop during low speeds and hence has a detrimental effect on developed electromagnetic torque at low speeds. Resistance and excitation levels affects acceleration time because they determine the amount of power discharged in the resistors during acceleration.

It is thus the conclusion of this section that the model is sufficiently accurate when parameters are accurate. The problems regarding excitation are only severe in the sense that they hinder the accurate replication of the shop model system. In full scale simulations a voltage controller is used and as long as it and its input to the generator is feasible there is no particular reason to believe that the results would not be feasible.

3.2 Simulation model updated parameters

In the pre-project, getting hold of parameters for Motorformers was a problem. However, exact data for a representative Motorformer has now been acquired at the courtesy of StatoilHydro. The machine is from the Troll A Pre-Compression project, and its parameters are rendered in table 3.2.

V_{rated}	= 58 kV
X_d	= 1.14
$X_d^{'}$	= 0.357
$X_d^{''}$	= 0.305
X_q	= 0.655
$X_q^{''}$	= 0.457
$T_d^{'}$	= 1.12
$T_d^{''}$	= 0.015
$T_q^{''}$	= 0.056
$R_{s,70}$	= 0.0014

Table 3.2.1: Per unit parameters for 45 MVA Motorformer

The interconnecting cable between the generator and motor is modelled as a PI-section line, with the same parameters used in section 4.1.1. In light of the results presented in section 3.1.5, simulations were conducted on a full scale drive, using updated parameters as presented in the above.

Low frequency starting

The system was successfully started using the low frequency starting method with interconnecting cable as long as 60 km. At this point, further work to increase cable length was regarded as being unrealistic and beyond the scope of work.

The PI-controller that fed the excitation signal to the motor, controlling it to run at unity power factor, had to be cut and the motor fed by constant excitation. This was due to oscillations in reactive power after the system had reached target speed, eventually resulting in the system loosing synchronism.

Figure 3.2.1 shows the generator and motor output reactive power and terminal voltage for a low frequency start at 60 km cable length. It is obvious that both machines are now receiving reactive power from the cable, and voltages reach higher levels accordingly. As mentioned in the above, the effective management of long sub sea cables is not within the scope of this thesis. However, it has been indicated that, given the validity of the simulation model, the starting concept is not limited by cable length within reason, but rather by conventional problems associated with long sub sea cables, i.e. the management of excess reactive power.

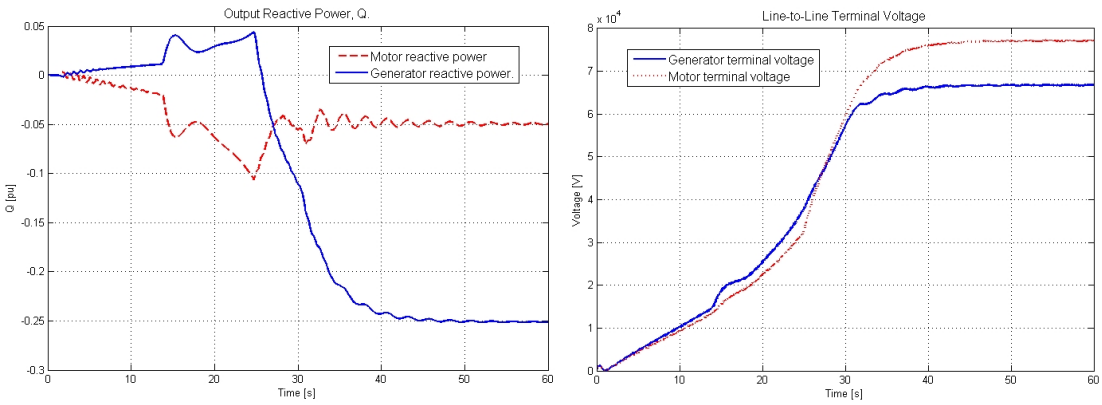

Figure 3.2.1: Generator and motor reactive power and terminal voltage for 60 km.

Partial frequency- and soft starting

In light of the discoveries made in the laboratory no serious attempts were made at partial frequency starting. Soft starting was attempted on the simulation model described in the above. The voltage controller was decoupled from the generator and the V_f input was ramped from 0 to 3 in 30 seconds, after which the excitation was kept constant for the duration of the simulation.

Due to switching problems in Matlab-Simulink, it is rather tricky to perform synchronization. However, it has been assumed that in the real world with professional equipment available, this is not a problem as long as the slip speed at which the attempt is made is not too high.

The longest line length at which soft starting was successful was 10 km. The minimum slip registered was 0.04 pu, or 60 rpm, and the speeds and voltages are shown in figure 3.2.2. It is assumed that synchronization is possible for this slip.

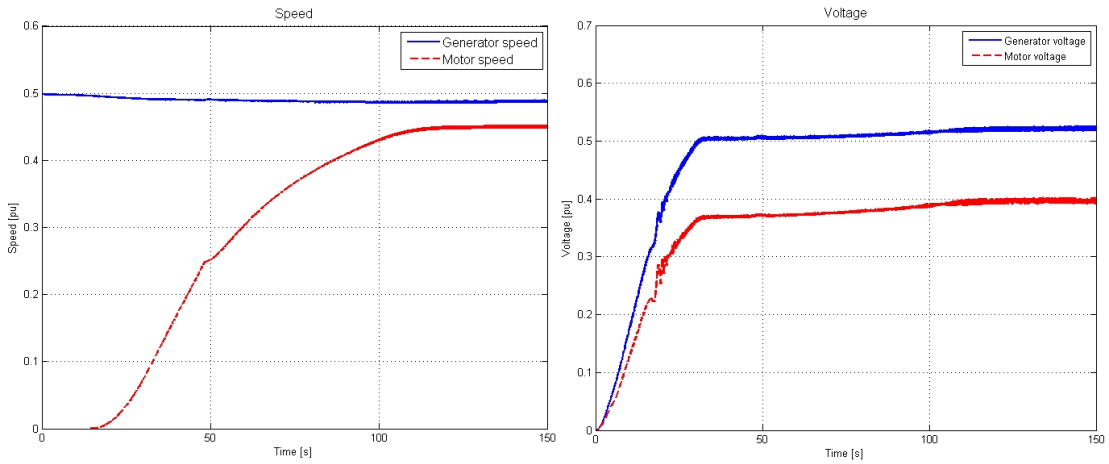

Figure 3.2.2: Generator and motor speeds (left) and voltages (right) for Soft start at 10km.

By closely inspecting figure 3.2.2, a knee in the acceleration curve of motor can be seen at approximately 50s. It occurs at a speed of almost 0.25 pu, which coincidentally means a slip of ≈0.5. The knee thus appears to be caused by the so called Gorges Phenomenon, and at higher line lengths, it limits the starting of the motor. The Gorges Phenomenon refers to a saddle in the developed asynchronous torque of a starting synchronous machine and is caused by counter rotating magnetic fields on the rotor surface [7]. It occurs around s=0.5 and the shape and depth of the saddle is governed by machine and power system resistance. The saddle is most pronounced in solid pole rotors and minimum in cylindrical rotors and laminated poles with the inclusion of damper windings. If the resistance had been zero, the saddle would disappear entirely [7]. This might explain why acceleration time appears sensitive to line length.

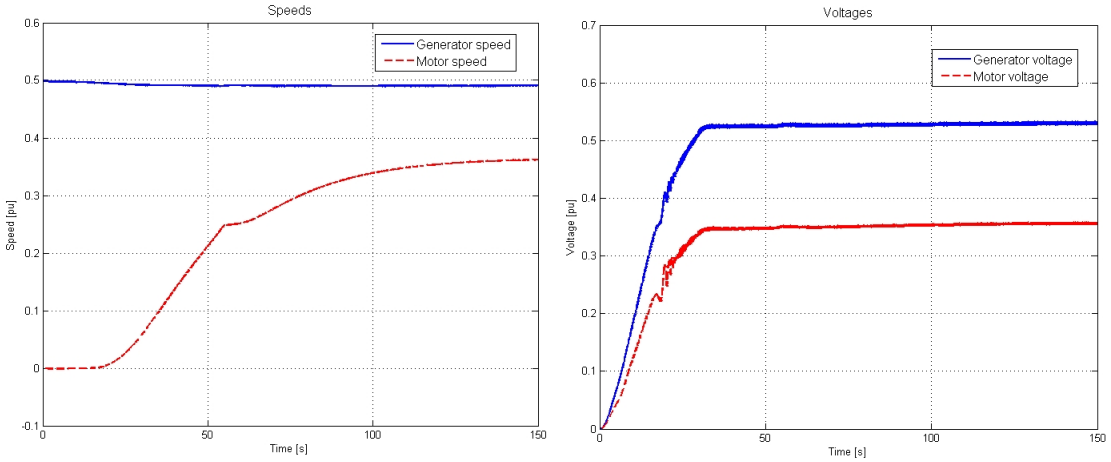

Figure 3.2.3: Generator and motor speeds (left) and voltages (right) for Soft start at 14km.

Figure 3.2.3 shows a soft start attempted at 14 km cable length. It can be seen that the transition to unfeasible line length is gradual, as it appears in increased minimum slip speed at which synchronization needs to be attempted and starting time. In the case of figure 3.2.3 the minimum slip is approximately 0.12 pu, or 180 rpm, and the start-up is thus deemed unsuccessful.

Thermal heating of the rotor is an issue that, unfortunately, there was no time to properly assess in this thesis. However, it is a mathematical property of the inertia constant that thermal heating during an unloaded start to synchronous speed is $H \cdot S$ [3]. Modifying H to correspond with reduced frequency and using the total inertia as calculated in sub-section 4.1.1 for the sub-cooling compressor drive, we get:

$$H_{reduced} = \frac{0.5 \cdot 13434.3(\frac{188.5}{2})^2}{65 \cdot 10^6}$$
$$E_{thermal} = H_{reduced} \cdot S$$
$$E_{thermal} = 59.66MWs$$

Dividing by the approximate starting time of 100s yields:

$$P_{cooling} = \frac{E_{thermal}}{t_{starting}}$$
$$P_{cooling} = 596.6kW$$

During normal operation the Sub-cooling compressor draws approximately 56 MW, thus the unloaded required cooling power druing soft start is approximately 1% of the load power at rated conditions. In comparison the Motorformer from which data has been used, has a cooling heat loss of 690 kW at rated operation of 44 MW, which translates into 2.18%. The actual maximum cooling capacity is not known to the author, but it is probably quite higher.

It has thus been indicated that unloaded cooling power required for soft starting is relatively small, but the effects of loading the compressor remains to be adressed. The thermal capacity of the rotor is a design issue and if the soft starting was to be chosen as the preferred starting method, machines could be custom designed to meet with requirements.

3.3 Availability of prime mover

For low frequency starting it is apparent that a mechanical prime mover with considerable torque at zero speed is required. As mentioned earlier, the torque-speed characteristics used in this the laboratory and simulations in this master thesis is from a GE LM 6000 [14]. The LM 6000 is an aero derivative two shaft gas turbine, and its construction is illustrated in figure 3.3.1.

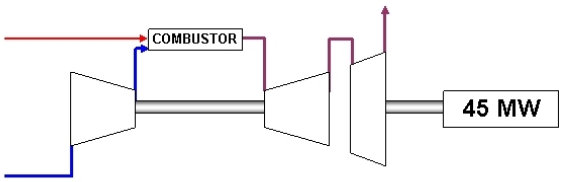

Figure 3.3.1: LM 6000 2 shaft gas turbine.

The LM 6000 marine gas turbine is available in power ratings up to approximately 42 MW [17]. A higher power alternative is the LMS 100. It is illustrated in figure 3.3.2 and is available in power ratings up to 104 MW at 3600 rpm [18].

According to General Electric, the LMS 100 demonstrated a breakaway torque of 40 kN [18]. During the test in question, the measurement equipment was the constraining factor, and the LMS 100 is hence assumed to be capable of even higher breakaway torques. For the compressor presented in section 2.1, which is regarded as a typical LNG sub-cooling compressor, the required breakaway torque is approximately 3 kN. This leaves a smooth 37 kN of accelerating torque.

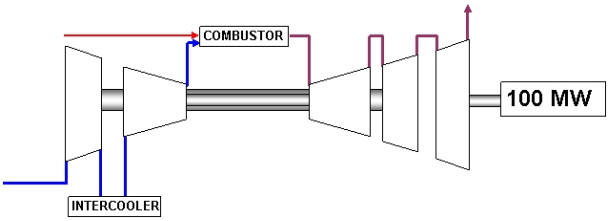

Figure 3.3.2: LMS 100 3 shaft gas turbine.

Figure 3.3.3 shows an example of a torque-speed characteristic of a typical steam turbine. It is rated at approximately 21 MW and has a drooping torque characteristic toward the second half of the speed range. It has not been verified to the author that steam turbines are capable of significant torque at zero speed, however figure 3.3.3 indicates that using steam turbines are perfectly suitable for the soft starting scheme.

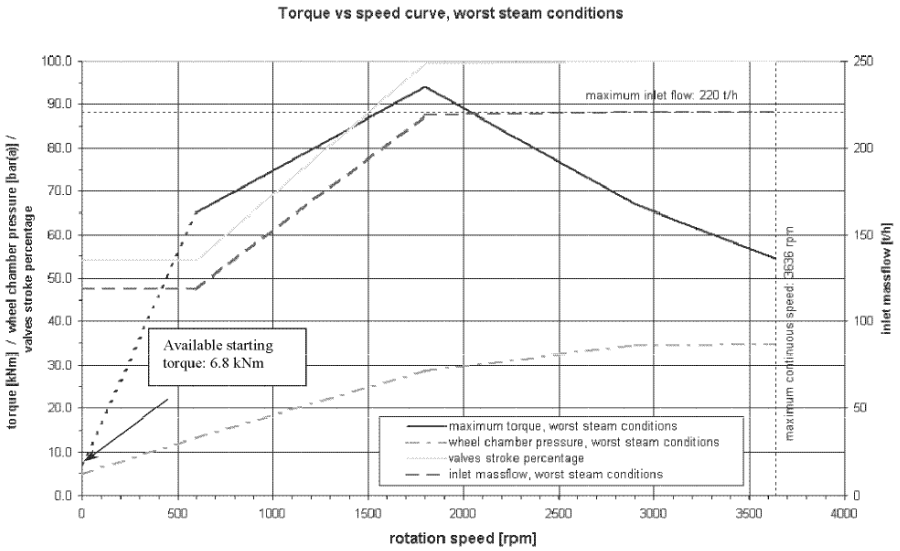

Figure 3.3.3: Typical torque-speed characteristic of a steam turbine.

3.4 Starting conclusions

In this section the Low frequency- and Soft starting will be assessed in light of the results from the laboratory and the simulations. The feasibility of the starting methods will evaluated and they will be compared to each other. In light of the results of the laboratory tests, partial frequency starting is not discussed. For a more a thorough explanation see sub-section 2.3.2

3.4.1 Low frequency starting

The main benefits of Low frequency starting is the relatively low currents involved in the starting procedure, as well as the absence problems concerning Gorges Phenomenon and thermal heating. The low starting currents means that the voltage drop across any line that might be connecting the two machines is minimized. Also, as the initial few hundred critical rpms has been negotiated, excitation control may be applied to the motor. In this manner reactive power can be handled in an intelligent way and, perhaps more relevant to the case, developed torque can be maximized.

Through exploration of the effects of resistance it was shown that as resistance is the dominating part of the impedance at low speeds, the voltage drop it causes can not be neglected. Once excitation levels have been adjusted appropriately, the effect of resistance boils down to available active power to feed losses, and hence is a matter of prime mover torque at the speed in question.

The main drawback of Low frequency starting is turbine torque at low speeds. In sub-section 3.1.4 is was shown that once excitation level were correct, the limiting factor was available prime mover torque. As discussed in section 3.3, the ability of larger turbines to produce torque at very low speeds is somewhat uncharted territory. However, it has been indicated that the LMS 100 has shown great promise.

The line resistance from terminal to terminal in the laboratory is quite extensive when considered in per unit, and even more so when considering that the available prime mover power is less than half of synchronous machine ratings.

3.4.2 Soft starting

The main advantage of the soft starting scheme is that mechanical torque availibility is not an issue because some 40-50% reduction in speed is sufficient to drastically reduce the quadratic load torque. The laboratory tests for soft starting conducted in this thesis was with the field winding open cirucited. It is assumed that with the ability to properly short circuit the field windings, even more promising results will appear.

In full scale simulations, the motor has been successfully started for line lengths exceeding 10km. As line length increases, the generators ability to produce torque at the motor side is weakened, and the slip at which synchronization is attempted increases.

The machines used in the simulations are salient pole, which not ideal for such purposes because they loose torque at as slip speed becomes small. The effects of the Gorges Phenomenon is evident in the simulations, a fact which lends credibility to the simulation models.

When soft starting the motor is started asynchronously. This means that the entire reactive power load must be taken by the generator and that it is bigger than in low frequency synchronous starting. The developed electromagnetic torque is dependant on the generators ability to produce voltage at the motor terminals and construction of the motors damper windings. If Soft starting is the chosen starting method, it is likely that machines will be custom designed for the application. If so, it should be possible to minimize the effect of the Gorges Phenomenon, which otherwise imposes constraints on starting. Thermal heating of the machines has only been briefly discussed, but it has been shown that the thermal heating during unloaded start is only 1% of machine power output at rated conditions. It is thus assumed that during design of the machines, the damper windings could easily be dimensioned for the entire load.

Chapter 4

Impact on running performance

In addition to the challenges regarding starting the compressor machines, the transition to fixed speed drives would entail consequences on the operability of an LNG-facility. Beforehand it may perhaps be assumed qualitatively that the currents in the event of a short circuit will be larger than in the LCI alternative, because the direct connected electric machines deliver currents to the fault, as opposed to an LCI-drive that blocks such current flows.

4.1 Dynamic simulation model

In order to investigate some of the effects of fixed speed drivers in an LNG-facility, a simulation model was established in SIMPOW.

4.1.1 System design.

The model comprises three generating units, a pre-cooling compressor, a sub-cooling compressor, liquefaction compressor and a N_2CH-compressor. The LNG-facility voltage level is 66kV and it is connected to the main power grid through a step up transformer and a 100km, 132kV transmission line. It is on this transmission line and on the transformer high voltage terminals that short circuit tests will be performed.

Machine parameters

Since Motorformer parameters are scarce, all machines have been modelled after the Troll A pre-compression machine, as described in section 3.2.

Inertia

The Troll A machine is rated at 45MVA, making its inertia unusable for our purposes. When scaling the machine to the ratings required, it has been assumed that the rating is changed by manipulating the rotor length, l, increasing the rotor inertia proportionally according to ([8], 2-7):

$$\begin{aligned} J &= r^2 \cdot dM \\ dM &= \rho \cdot r d\theta \cdot dr \cdot dl \end{aligned}$$

This gave the following equivalent inertias: Consequently, the machine inertia constant,

	Pre-cooling	Sub-cooling	Liquefaction	N_2CH
J	9434.3	13434.3	11333.8	NA

Table 4.1.1: Equivalent inertias according to gear ratios

H, is assumed to be preserved as rating and inertia is increased:

$$\begin{aligned} H &= \frac{0.5 J \omega_r^2}{S_n} \\ H &= c_1 \frac{c_2 l}{c_3 l} \end{aligned}$$

In this manner the scaled rotor inertia was determined, to which the compressor inertia was added after being corrected for gear exchange ratio, n:

$$J_{eq} = J_r + J_c \cdot n^2 \tag{4.1}$$

Thus, new equivalent machine and compressor inertia constants could be calculated. They are shown in table 4.1.2 together with those of the generators. Due to lacking data for the N_2CH compressor, it was assumed that it had the same per unit inertia that of the liquefaction compressor. Also the gas turbines have been neglected in calculating the generator inertia constants, due to lack of data.

Grid details

The voltage level in the internal grid LNG-facility was set to 66 kV and is assumed to consist of paralleled ground cables, while the overhead transmission line was set at 132 kV. The line and cable specifications are rendered in table 4.1.3. All data in table 4.1.3 is obtained from [19].

	Generators	Pre-cooling	Sub-cooling	Liquefaction	N_2CH
H	2.25	2.58	3.67	6.29	6.29

Table 4.1.2: Inertia constants

	Type	$R[\Omega]$	$X[\Omega]$	$C_d[\mu F]$	$I_{th}[A]$	$I_k[kA]$
Cables	TSLE $2 \cdot 1 \cdot 800$	0.0185	0.08	0.56	1560	144
Line	FeAl $1 \cdot 506/1$	0.395	0.415	$8.8e^{-3}$	362	NA

Table 4.1.3: Line and cable specifications.

At the end of the transmission line there is an infinite bus modelling a stiff grid, maintaining 132 kV. A step down transformer and a resistive load has been included in order to address that the machines are not the only loads in the system, but any further analysis into what happens at the auxiliary voltage levels has been deemed beyond the scope of work.

The rated frequency was set to 60 Hz because this corresponded with rated data for machines and compressors. While a grid connection seems and 60 Hz operating frequency seems far-fetched outside of North-America, it is easy to imagine that the machines in question may be designed for 50 Hz operation or that the can be operated at this frequency. As for the compressors that are rated at 3600 rpm, it has been assumed that they could be geared at a ratio of 2. If this is the case then it is not unlikely that they can be geared at a ratio of 2.4. The transformer interfacing the transmission line is rated

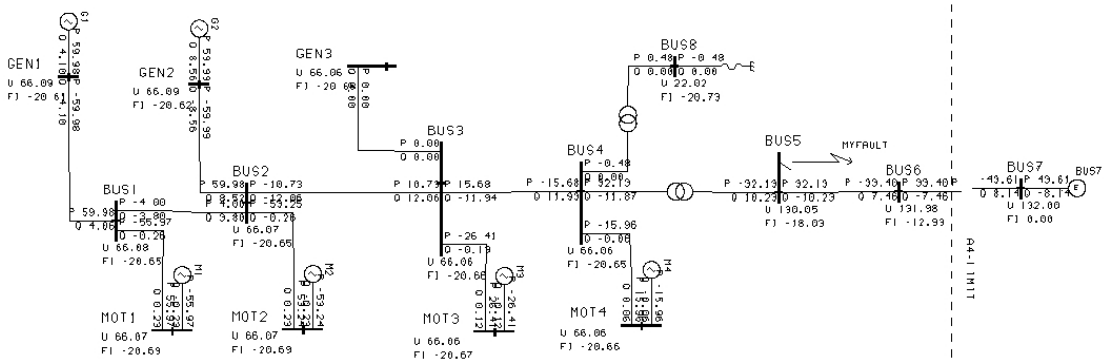

Figure 4.1.1: Single line diagram of fixed speed LNG facility.

at 100 MVA and the short circuit reactance was set to 15%. This might be slightly on the high side, but similar values has been used LNG facility short circuit calculations before [20] and is thus not outrageously controversial.

Turbine and governor model

The model used is a simplified gas turbine/diesel engine model found in the SIMPOW library. It consists of a transport- and time delay in series, as can seen in figure 4.1.2. Its input is gate opening Y and its output is torque T_m. The governor is also a simplified model, consisting of a speed feedback loop with a speed control gain and a time delay. A schematic of the governor can be seen in figure 4.1.3.

Some attempts to obtain representative parameters for these models were made, but

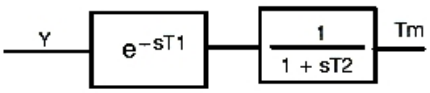

Figure 4.1.2: Turbine model.

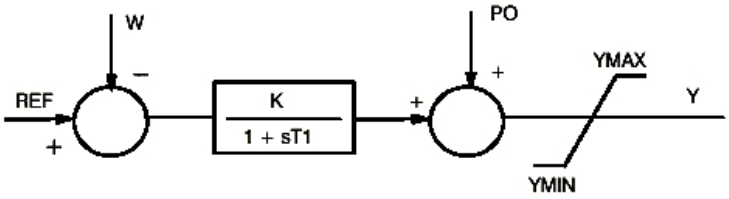

Figure 4.1.3: Turbine governor model.

quickly abandoned as it is well beyond the scope of this thesis and because their effect on the system performance were shown to be minimal. Instead some parameters were chosen that did not seem unreasonable to the author and his adjutants. They are:

Governor:	K = 1	T1 = 0.02
Turbine:	T1 = 0.1	T2 = 0.1

Mechanical loads

The loads torque-speed tables of representative LNG-compressors in per unit of machine ratings. There are three unique tables; pre-cooling, sub-cooling, and liquefaction compressor loads. For the N_2CH compressor it was assumed that the per unit torque-speed characteristic was identical to that of the liquefaction compressor. Again this was due to lack of data.

4.2 Short circuit analysis

The systems behaviour during short circuit was explored, in order to determine the consequences of introducing fixed speed motor drives.

4.2.1 Three-phase to ground

A series of three-phase to ground short circuit simulations were done on the line interconnection the grid and the LNG-facility. The duration of the faults was 350ms and the point of fault was gradually moved closer to the transformer while the currents were logged. This included the peak short circuit current and the peak second swing current for the transformer, motors, and generators, as well as the minimum motor terminal

L	$I_{k,trafo}$	$U_{min,m2}$	$I_{k,m2}$	$I_{s.swing,m2}$
100	2.262	0.832	0.563	1.809
90	2.41	0.821	0.562	1.826
80	2.579	0.809	0.558	1.846
70	2.773	0.796	0.555	1.865
60	3	0.781	0.551	1.882
50	3.268	0.763	0.547	1.897
40	3.595	0.743	0.541	1.904
30	3.995	0.719	0.533	1.892
20	4.503	0.691	0.524	1.838
10	5.227	0.659	0.521	1.685
0	6.26	0.621	0.552	1.327

Table 4.2.1: Short circuit currents for interconnecting transformer and motor.

voltage was recorded. In table 4.2.1 one may observe minimum voltage, short circuit current, and second swing current for motor 2, that is the sub-cooling compressor drive, as well as the transformer short-circuit current.

From table 4.2.1 it can be seen that, as expected, the transformer short circuit currents increase with decreasing line length. However, the motor short circuit current and - second swing current decreases as the line length decrease. Also, the actual motor short circuit currents are fairly small compared to the total short circuit currents and the second swing current. The IEC standard states that the protective devices on motors should be set to limit the continuous. However, most notably we can see that largest voltage dip, at 0.621 pu, does not cause the machines to loose synchronism. Figures 4.2.1 and 4.2.2 shows the motor 2 speed and terminal voltage after a short circuit on the transformer high voltage terminals. From it, it can be seen that the motor speed swing has an amplitude of almost 1%, translating into 36 rpm at the compressor side, and that, due to voltage governor action the voltage is restored to ≥ 0.8 pu after approximately 100-150 ms.

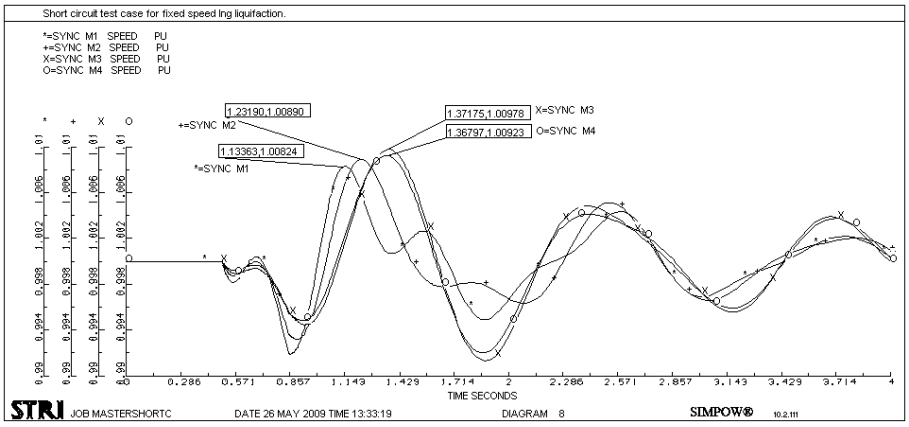

Figure 4.2.1: Motor speeds after three phase short circuit on transformer high voltage side.

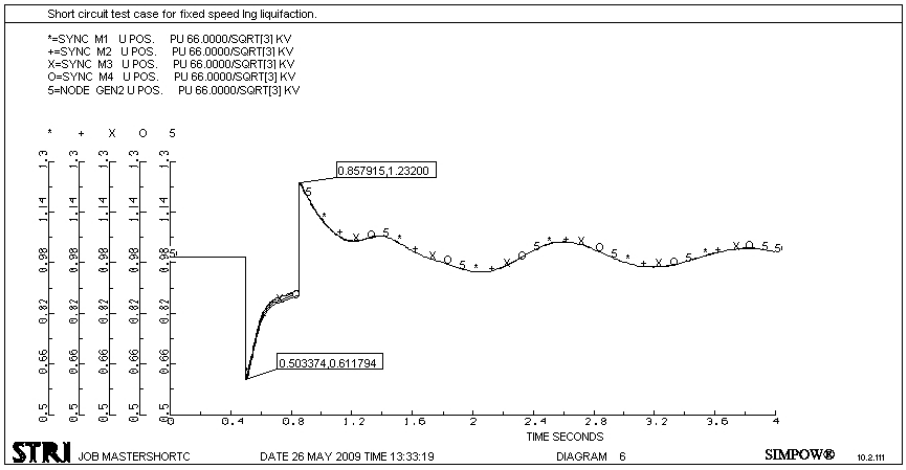

Figure 4.2.2: Motor terminal voltages after three phase short circuit on transformer high voltage side.

L	$I_{k,trafo}$	$I_{k,g1}$	$I_{s.swing,g1}$	$I_{k,g1}$	$I_{s.swing,g1}$
100	2.262	1.404	1.621	1.443	1.721
90	2.41	1.462	1.653	1.504	1.755
80	2.579	1.531	1.685	1.574	1.783
70	2.773	1.611	1.708	1.659	1.812
60	3	1.707	1.726	1.759	1.828
50	3.268	1.824	1.726	1.88	1.829
40	3.595	1.968	1.701	2.031	1.804
30	3.995	2.15	1.638	2.218	1.714
20	4.503	2.385	1.519	2.463	1.622
10	5.227	2.702	1.32	2.793	1.424
0	6.26	3.294	NA	3.177	NA

Table 4.2.2: Short circuit currents for interconnecting transformer and generators

Taking a look at the generator currents in table 4.2.1, it can be seen that the tendency is opposite for the short circuit currents, while the second swing currents also decrease with decreasing line length.

Figure 4.2.3 shows the generator and transformer currents in the event of a three-phase with ground fault on the transformer high voltage terminals. It can be seen that as the AVR acts to re-establish the voltage, the fault current is worsened. In the event of such a severe fault, causing voltage drops down 60% of nominal value and resulting currents of over 6 pu, it is reasonable to assume that protection equipment will be tripped, causing the system to shut down. It has, however, been demonstrated that, for the conditions described in section 4.1.1, the fixed speed motors are not the constraining factor in the event of such a scenario.

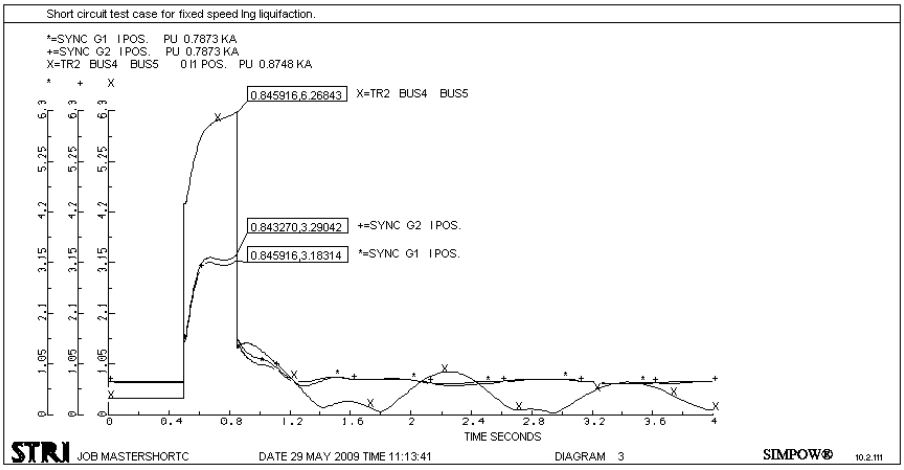

Figure 4.2.3: Generator and transformer currents for 3psg fault on transformer high voltage terminals.

4.2.2 One-phase to ground

At the request of StatoilHydro, a simulation of a one-phase to ground fault at one of the generators was done. The fault impedance was zero and the fault occurs at generator 1. The fault occurs at t=0.5s and is removed after 350ms by tripping the line from node GEN1 to BUS1. Figures 4.2.4, 4.2.5, 4.2.6 shows the node voltages, motor speeds, and generator currents after a one-phase to ground fault on GEN1.

From figure 4.2.4 it is evident that the voltage drop is approximately 7%, well within the 20% requirements in [21]. In figure 4.2.5 it can be seen that the highest peak speed swing is limited to 0.32%, corresponding to 11.52 rpm, for the liquefaction compressor. As for currents, the load is now split between the remaining generator and the incoming transformer after the fault is cleared. Figure 4.2.6 shows that the transformer bears the main brunt of the post fault loading, while the generator current hardly surpasses 1 per unit. It should be noted that the modelling of the grid connection does not include a Thevenin impedance, and is as such not necessarily good enough to representatively describe a post fault situation where only one generator is operating. However, the purpose of these simulations was not to investigate a grid driven LNG-facility, but rather to get an idea of how a fixed speed LNG-facility behaves under fault conditions.

4.3 Surge

Surge is an operating state for a compressor in which the peak head capability and minimum flow limits are reached [22]. The phenomenon is related to stall in an airfoil and when surge occurs the compressor looses it's capability to maintain head and it becomes unstable. Under normal operating conditions the compressor usually operates to right of, i.e. at higher flow than, the surge line. However, it may slip into surge during emergency stop or other conditions that causes flow to decrease [22].

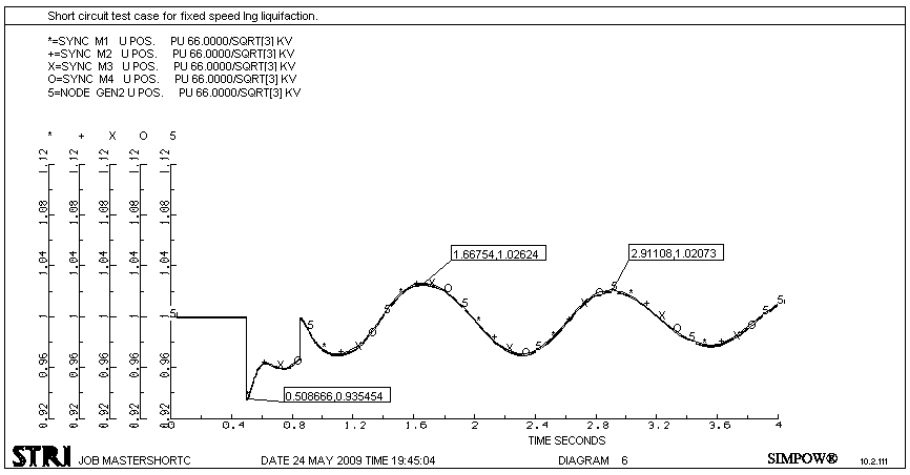

Figure 4.2.4: Node voltages after 1psg fault at GEN1.

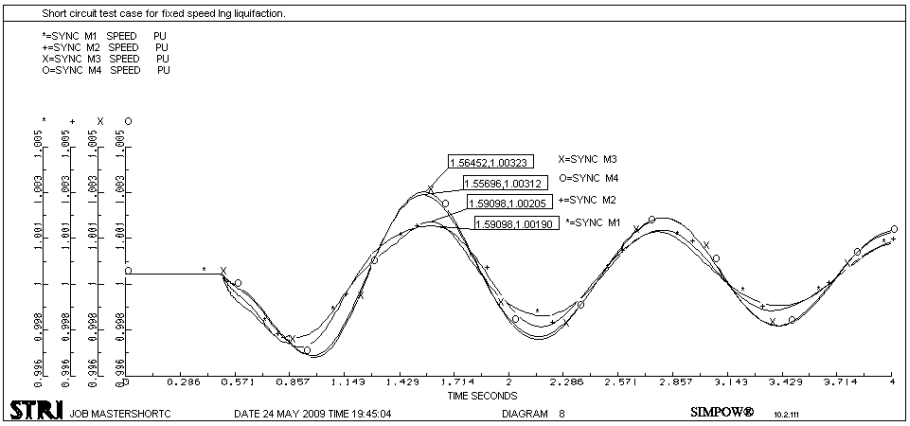

Figure 4.2.5: Motor speeds after 1psg fault at GEN1.

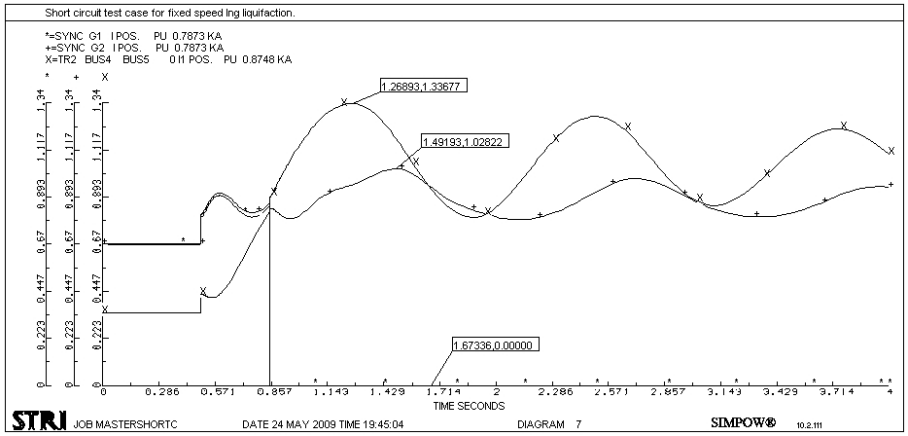

Figure 4.2.6: Generator currents after 1psg fault at GEN1.

There was concern that fixed speed compressor drives would increase the systems vulnerability to surge during fault situations. Surge, being a mechanical or gas dynamic phenomenon, is not within the authors field of expertise. However, as the results of the short circuit simulations were presented to Prof Lars Eirik Bakken of the Department of Energy and Process Engineering at NTNU, he stated that a peak swing of 1% hardly would result in any surge.

Figure 4.3.1 shows three useful ways of looking at surge: N vs Q, H vs N^2, and H vs Q^2. Upon inspecting the H vs N^2 curve in figure 4.3.1, it is evident that a large change in speed will bring the compressor to the left of the surge line as indicated.

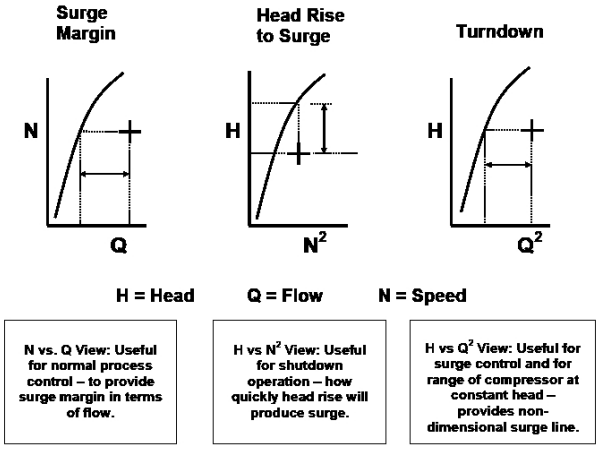

Figure 4.3.1: Three views of surge phenomenon.

4.4 LCI comparison

It could be the case that the fixed speed drive system is more robust than its variable speed alternative, the LCI drive. At Kollsnes gas processing facility on the west coast of Norway, the LCI drives were initially designed to reaccelerate if a voltage dip lasts for more than 500 ms [23]. However, the LCI-drive looses speed very quickly during a voltage dip below 80% of nominal value. This is because a dip of this scale will cause blocking of the Thyristors and the LCI will loose its torque almost instantly [23]. In comparison the fixed speed compressor motor will produce a transient torque dependant on its construction, in the case of a salient pole machine with laminated poles such as the Motorformer in question we have ([11], 154):

$$T_e = T_{E_q'}(\delta') = \frac{1}{\omega_s}\left[\frac{E_q' V_s}{x_d'}\sin\delta' - \frac{V_s^2}{2}\frac{x_q - x_d'}{x_q x_d'}\sin 2\delta'\right] \tag{4.2}$$

As long as there is a certain voltage within the LNG-facility grid, the motors will produce a torque. In addition the motors help keeping up the voltage within the facility by feeding the fault with reactive power. At Kollsnes the design was modified to enable

reacceleration after dips shorter than 150 ms. In comparison, all faults conducted in this study had a duration of 350 ms.

While the fixed speed solution might provide a more robust solution, it is at the cost of flexibility. Fixed speed entails a loss of tuning ability for the sake of the process and when using LCI-drives the ability to restart is present without any effort worth mentioning. On the other hand, the fixed speed alternative will, regardless of what starting scheme is chosen, be quite cumbersome to restart.

4.5 Running performance conclusions

The motors deliver current to the short circuit when they are directly connected to the grid, but their contribution is small compared to that of the generators. A 350ms full three-phase with ground short circuit on the high voltage terminals of the incoming transformer results in a voltage drop to approximately 60% of nominal value. This does not cause the motors to loose synchronism and voltage is quickly restored to $\geq$80% of nominal value, due to AVR action.

Peak transformer short circuit current for three-phase with ground fault is 6.26 pu, in the case of short circuit at transformer high voltage terminals. A 350ms one-phase to ground fault at a generator bus, with ensuing disconnection of the generator results in a motor terminal voltage drop of $\leq$ 7%. None of the machines loose synchronism and peak post fault speed oscillation amplitude is $\leq$ 0.4%. It is expected that through more sophisticated excitation control of the motors, the short circuit performance of fixed speed drives can be improved further. Sannino et. al. suggests a grid solution for an LNG facility where the incoming transformer is replaced by a current limiter [20]. Such a scenario, where the effective short cirucit impedance between the LNG-grid and the transmission line is increased to 32%, could also be realistic in a fixed speed solution. The transmission line could then be at the same voltage as the motorformers constituting motor drives and generators.

The danger of surge can not be written off, but it appears to be less than or equal to that in the LCI-alternative. This is due to the fixed speed alternatives ability to maintain a certain torque during voltage dips. Gas dynamic phenomena are not the theme of this thesis, a more thorough study into the consequences for the process is needed.

Chapter 5

Conclusions and Further work.

5.1 Fixed speed LNG conclusions

The feasibilty of the loaded Back-to-Back synchronous- and soft starting schemes for drives in laboratory rating class seems thoroughly proved. Regarding the scalability of the laboratory runs, extensive investigations have been made into the validity of the simulation model on which full scale simulations have been conducted. The simulation model appears to be reasonably accurate, given accuracy of its input parameters. There were difficulties in translating field currents into per unit field voltage for the simulation model. This caused discrepancies in the resulting line voltages. It appears that the conditions under which laboratory start-ups were performed is rather unfavourable with regards to resistance when compared to a full scale scenario. Resistance seems to be an important parameter, due to its domination under low frequencies.

Assuming validity, the full scale simulations shows great promise. The low frequency starting scheme, not being limited by any remotely realistic cable length, appears to be the most reliable. It is also the least violent starting scheme in all facets of the problem. Low frequency starting is mainly limited by available torque at low speeds, which is an issue that has not been clarified. Though most beneficial at a somewhat reduced speed, soft starting is not bound by the torque availability problem as it can be performed at any speed and steam turbines are readily available with certain speed reduction capabilities.

The investigation into the impacts on grid conditions are not detailed enough to draw final conclusions on feasibility. However, it has been indicated that short circuit performance of the internal LNG-facility grid can be improved by switching to fixed speed motor drives. Severe faults were imposed on the system without loss of synchronism. Though not verifiably, it appears that the system is more robust against problems relating to surge. The speed swings are in order of magnitude 1% or less. However, even if the fixed speed solution should entail an increased robustness, the consequences of loss of synchronism is much greater than tripping of the LCIs in a variable speed system. This is because, as has been indicated in the previous chapters, the starting process of a fixed speed compressor drive is quite complex. The loss of synchronism would almost

surely lead to a halt of the entire system.

In final, it is the conclusion of this thesis that Fixed Speed LNG appears perfectly feasible from an electric power engineering perspective. The desirability of the fixed speed solution is then wholly dependant on the process' need to adjust compressor speed, and on the availibility of prime movers with considerable torque capability at zero and low speeds.

5.2 Further work

The scope of this thesis has, over the course of the semester, become quite extensive. As a consequence it has on several occations been necessary to limit the work and refer the issue at hand to further work. In the following an account will be made of the themes that, in the opinion of the author, are in need of closer scrutiny.

An experimental account of compressors in the 6 kW range has been made. The next natural step would now seem to be scale up the experiment. It has been concluded that, provided mechanical torque availability, this should be easier than in small scale. It is neccessary verify the availability of torque at low speeds.

The discrepancies in voltage due to faulty assumptions on field current in the simulation modell will have to be improved. A detailed simulation model featuring sophisticated synchronous machine models, capable of accurate simulation of the larger-scale experiment in the above should be established in order to minimize project risk. Control systems will have to be developed for turbine- and excitation control during starting.

The effects of resistance on soft starting and how it relates to Gorges Phenomenon should be investigated. More accurate assessments on thermal heating during soft starting should be performed.

Preliminary custom design work on Motorformers for fixed speed LNG application should be conducted. The nature of this work will depend on what starting scheme is chosen. In the case of soft-starting, it will be necessary to design damper windings to minimize the effects of Gorges Phenomenon.

The studies into grid performance that made in chapter 4 are quite shallow. A multitude of features remains to be studied and the work performed in this thesis needs to be controlled. A comprehensive grid design should be made, featuring a representative incoming transformer or current limiter, voltage levels, and protection equipment.

Bibliography

[1] F. Christiano M. Harrison S. Shu. Analysis points to electric-motor drivers for angola lng. *Oil and Gas Journal*, 100(40):60, 2002.

[2] F. Kleiner S. Kauffman. All electric refrigeration compressors in lng plants offer advantages. In *Gastech*, 2005.

[3] M. Kazi. Practical requirements for starting very large machines. In *IEE Colloquium on Design, Operation and Maintenance of High Voltage Electric Motors for Process Plant*. IEEE, 1999.

[4] C. Concordia P.G Brown W.J. Miller L. Wuosmaa. Synchronous starting of motor from generator of small capacity. *IEEE Transactions on power apparatus and systems*, 86(10):1215, 1967.

[5] W. Garret E.A. Groscup R.T. Cooper E.Byerly C. Whitney J.P. Fitzgerald. Synchronous starting of seneca pumped storage plant. *IEEE Transactions on power apparatus and systems*, 88(4):307, 1969.

[6] D. N. Konidaris. Investigation of back-to-back starting of pumped storage hydraulic generating units. *IEEE Transactions On Energy Conversion*, 17(2):273 – 278, 2002.

[7] J. Casey J.C Das. Characteristics and analysis of starting of large synchronous motors. In *Industrial and Commercial Power Systems Technical Conference*. IEEE, 1999.

[8] N. Mohan. *Electric Drives - An integrative approach*. MNPERE, 3 edition, 2003.

[9] H. Breistein. On-load starting of synchronous machine compressor drives. Available at Department of Electric Power Engineering, NTNU. Energy Conversion Group., 2008.

[10] P. Kundur. *Power system stability and control*. McGraw-Hill, 1993.

[11] J.W. Bialek J.R Bumby J. Machowski. *Power System Dynamics and Stability*. Wiley, 1997.

[12] G. Champenois S. Tnani E. Mouni. Synchronous generator modelling and parameters estimation using least squares methor. *Simulation Modelling Practice and Theory*, 16:678–689, 2008.

[13] C. Kingsley S.D. Umans A.E. Fitzgerald. *Electric Machinery*. McGraw-Hill, 5 edition, 1992.

[14] F. Kleiner S. Kauffman. Lm6000 pc/pd gas turbine for mechanical drive applications. In *2nd Gas Turbine Symposium*, 2003.

[15] Inc The MathWorks. *Matlab Manual*, 2008.

[16] I.M Canay. Discrepancies of rotor quantitites and exact equiavalent diagrams. *IEEE Transactions on Power Apparatus and systems*, 88(7):1114, 1969.

[17] GE Marine. Lm 6000 marine gas turbine datasheet., 2006.

[18] General Electric. Test results lms 100 torque capability, 2008.

[19] Sintef. *Planleggingsbok for kraftnettet Bind 3.*, 2003.

[20] A. Sannino. All-electric lng liquefaction plants. technical challanges possible concept solutions. In *Industry Applications Conference, 2007. 42nd IAS Annual Meeting*, 2007.

[21] IEC 61892-1. International standard - mobile and fixed offshore units - electrical installations, 2001.

[22] K. Brun G. N. Marybeth. Application guideline for centrifugal compressor surge control systems, 2008.

[23] R. A. Roberton A. H. Børnes. Adjustable-frequency drive system for north sea gas pipeline. *IEEE Transactions on Industry Applications*, 34(1), 1998.